Report no. changed (Mar 2006): SM-219-UU

SACLANTCEN MEMORANDUM
serial no.: SM-219

SACLANT UNDERSEA
RESEARCH CENTRE

MEMORANDUM

Delay-Doppler resolution performance of large time-bandwidth product linear FM signals in a multipath ocean environment

J.-P. Hermand
and W.I. Roderick

April 1989

The SACLANT Undersea Research Centre provides the Supreme Allied Commander Atlantic (SACLANT) with scientific and technical assistance under the terms of its NATO charter, which entered into force on 1 February 1963. Without prejudice to this main task – and under the policy direction of SACLANT – the Centre also renders scientific and technical assistance to the individual NATO nations.

This document is released to a NATO Government at the direction of SACLANT Undersea Research Centre subject to the following conditions:

- The recipient NATO Government agrees to use its best endeavours to ensure that the information herein disclosed, whether or not it bears a security classification, is not dealt with in any manner (a) contrary to the intent of the provisions of the Charter of the Centre, or (b) prejudicial to the rights of the owner thereof to obtain patent, copyright, or other like statutory protection therefor.
- If the technical information was originally released to the Centre by a NATO Government subject to restrictions clearly marked on this document the recipient NATO Government agrees to use its best endeavours to abide by the terms of the restrictions so imposed by the releasing Government.

Page count for SM-219
(excluding covers)

Pages	Total
i–vi	6
1–19	19
	25

SACLANT Undersea Research Centre
Viale San Bartolomeo 400
19026 San Bartolomeo (SP), Italy

tel: 0187 540 111
telex: 271148 SACENT I

NORTH ATLANTIC TREATY ORGANIZATION

Report no. changed (Mar 2006): SM-219-UU

SACLANTCEN SM-219

Delay-Doppler resolution performance of large time-bandwidth product linear FM signals in a multipath ocean environment

J.-P. Hermand and W.I. Roderick

The content of this document pertains to work performed under Project 02 of the SACLANTCEN Programme of Work. The document has been approved for release by The Director, SACLANTCEN.

Issued by:
Systems Research Division

J. Marchment
Division Chief

Report no. changed (Mar 2006): SM-219-UU

intentionally blank page

Report no. changed (Mar 2006): SM-219-UU

Delay-Doppler resolution performance of large time-bandwidth product linear FM signals in a multipath ocean environment

J.-P. Hermand and W.I. Roderick

Executive Summary: The primary function of active sonar systems in ASW is to detect and localize submarines. In localization the key target parameters to be determined are range and range rate, which are derived from the measured travel time of the transmitted pulse and its Doppler shift respectively.

The range determination requires *short* pulses equivalent to *large frequency bands*, whereas range rate determination requires *long* pulses. Both can be achieved simultaneously by applying so-called 'large time-bandwidth product' pulses. The most common one, also used in radar, is the chirp pulse which changes frequency linearly during the time of pulse transmission and is called a 'linear frequency modulated' or LFM pulse.

As long as there is a single propagation path between sonar and target, range and range rate can be determined by conventional signal processing techniques. However, under conditions of multipath propagation, the received echo will consist of several pulses. If they overlap in time the multipath propagation can severely limit the range and range rate determination.

Since the present LFM pulses applied in sonar systems generally employ a relatively small time-bandwidth product the performance limitation of large time-bandwidth product LFM signals has not been extensively studied, especially in a multipath environment.

This study quantifies the errors that result when determining range and range rate in a multipath environment using large time-bandwidth product or LFM pulses. It is demonstrated via computer simulation that conventional processing, in fact, can give incorrect range and range rate information when overlapping multiple returns are received. The errors are described in terms of the parameters of the large time-bandwidth product pulse. Finally, a processing technique to determine the true range and range rate is suggested and demonstrated by simulation. The technique is shown to work well at high signal-to-noise ratios.

Future work will address the development of improved processing techniques to deal with lower signal-to-noise ratios. Also, actual at-sea data will be analysed to verify the computer simulation.

Report no. changed (Mar 2006): SM-219-UU

intentionally blank page

Report no. changed (Mar 2006): SM-219-UU

Delay-Doppler resolution performance of large time-bandwidth product linear FM signals in a multipath ocean environment

J.-P. Hermand and W.I. Roderick

Abstract: Active sonar systems that transmit large time-bandwidth (TW)-product linear frequency modulated (LFM) waveforms and receive echoes from targets of unknown range and speed can suffer considerable correlation losses that cannot be predicted from conventional (narrow-band) ambiguity function theory. As is well known, the theory can be modified to include the effects of Doppler distortion on large TW-product signals by correlating the received signal against a reference that is a time-compressed version of the transmitted signal. In this article, the effects of multipath (or target highlight structure) and Doppler on the correlation process for rectangular-weighted large TW-product LFM waveforms are examined. Gaussian-weighted waveforms are also considered to examine sidelobe behavior. It is shown that in a multipath environment, the correlator output peak does not generally occur at the correct Doppler reference channel. This is due to the constructive/destructive interference of the summation of complex delay-Doppler autocorrelation functions associated with each return. A summation technique that identifies the appropriate Doppler reference channel is proposed; this technique allows the target parameters to be estimated if the signal-to-noise ratio is sufficiently high.

Keywords: active sonar ○ ambiguity function ○ correlation loss ○ Doppler ○ large time-bandwidth ○ linear frequency modulation ○ multipath ○ sidelobe ○ target localization ○ time compression

Report no. changed (Mar 2006): SM-219-UU

Contents

Introduction *1709*
I. Characterization of the target reflected signal *1711*
II. Range and radial velocity estimation *1711*
A. Correlation receiver *1711*
B. Autoambiguity function *1712*
III. Doppler-multipath model *1712*
IV. Application to the linear FM pulse *1713*
A. Rectangular-weighted LFM pulse *1713*
B. Narrow-band case *1713*
C. Large TW-product case *1714*
V. Two-path problem *1718*
A. Narrow-band case *1718*
B. Large TW-product case *1719*
VI. Numerical examples *1720*
A. One-path case *1720*
B. Two-path case *1721*
C. Four-path case *1721*
D. Gaussian-weighted reference *1722*
E. Summation technique *1723*
VII. Conclusions *1724*

Appendix – Derivation of $\Phi_i(\lambda_i, \eta)$ for large TW-product LFM pulses *1725*

References *1727*

This memorandum is reprinted from the *Journal of the Acoustical Society of America*, **84**, 1988: 1709–1727.

Delay-Doppler resolution performance of large time-bandwidth-product linear FM signals in a multipath ocean environment

Report no. changed (Mar 2006): SM-249-UU

Jean-Pierre Hermand
SACLANT Undersea Research Centre, Viale San Bartolomeo, 400, I-19026 La Spezia, Italy

William I. Roderick
Naval Underwater Systems Center, New London, Connecticut 06320

(Received 15 April 1988; accepted for publication 22 July 1988)

Active sonar systems that transmit large time-bandwidth (TW)-product linear frequency modulated (LFM) waveforms and receive echoes from targets of unknown range and speed can suffer considerable correlation losses that cannot be predicted from conventional (narrow-band) ambiguity function theory. As is well known, the theory can be modified to include the effects of Doppler distortion on large TW-product signals by correlating the received signal against a reference that is a time-compressed version of the transmitted signal. In this article, the effects of multipath (or target highlight structure) and Doppler on the correlation process for rectangular-weighted large TW-product LFM waveforms are examined. Gaussian-weighted waveforms are also considered to examine sidelobe behavior. It is shown that in a multipath environment, the correlator output peak does not generally occur at the correct Doppler reference channel. This is due to the constructive/destructive interference of the summation of complex delay-Doppler autocorrelation functions associated with each return. A summation technique that identifies the appropriate Doppler reference channel is proposed; this technique allows the target parameters to be estimated if the signal-to-noise ratio is sufficiently high.

PACS numbers: 43.60.Gk, 43.30.Es, 43.30.Vh

INTRODUCTION

Long-range detection, localization, and classification of targets by low-frequency active sonar systems can be subject to severe performance limitations. Reduced radiated power levels inherent in low-frequency transduction, ambient noise, boundary reverberation, and associated lower directivity of low-frequency receiving apertures necessitate improving overall system figure-of-merit by increasing the time-bandwidth (TW) product of the transmitted signal. Under noise-limited conditions, detection performance increases with signal energy, whereas, under reverberation-limited conditions, performance is additionally dependent on both signal duration and bandwidth. Achievable high TW products are subject to system and medium constraints, and a knowledge of the target characteristics.

Ideally, in an additive white-noise background, a correlation receiver processes the received signal against a reference signal that "best matches" the incoming echo. Alternatively, since the target signature, motion, and medium propagation effects are not known *a priori*, the echo return would be processed serially against a family of reference signals that represents all possible echo returns. The reference signals would account for target aspect highlight structure, cover the full range of expected target radial velocities and its variations over the signal duration, and include multipath propagation effects appropriate to the *in situ* environmental conditions. However, in practice, a reference channel is designed solely for a signal that is reflected from a constant-velocity point target and propagates over a single path. The reference channels differ from one another by Doppler compensation to account for different anticipated target velocities.

For given target and environmental conditions, the resolution performance of the correlation receiver, in delay and Doppler, can be described in terms of the ambiguity function. This ambiguity function indicates the accuracy to which a target's range and radial velocity can be estimated and this is dependent on the waveform characteristics of the transmitted signal. In essence, if the signal is narrow band, then the conventional (Woodward) formulation of the ambiguity function is appropriate.[1] For this narrow-band case, the exact effects of reflection from a moving point target, i.e., a time compression of the waveform for approaching targets and an expansion for receding targets, are approximated simply as a carrier-frequency (f_c) shift of the transmitted waveform. The assumption is that the modulation function is narrow band and is unaffected by the Doppler effect. The correlation receiver, for narrow-band waveforms, has reference signals that are carrier-frequency-shifted versions of the transmitted signal.

In this study, a "wideband" ambiguity function has been formulated for transmitted waveforms that have TW properties for which the effects of target motion must be included in both the carrier frequency and the modulation function. These effects can be taken into account in the correlation receiver by having reference signals that are time-compressed (and -expanded) versions of the transmitted signal.

The transmitted waveform does not have to have a very

 0001-4966/88/111709-19$00.80 © 1988 Acoustical Society of America

Report no. changed (Mar 2006): SM-219-UU

large fractional bandwidth W/f_c nor does the target have to have high velocity for there to be substantial differences between the narrow-band and wideband properties of the ambiguity function. This is particularly true for the Doppler tolerances of large TW-product linear frequency modulated (LFM) waveforms. Harris and Kramer[2,3] asymptotically evaluated the ambiguity function for the effects of Doppler distortion on large TW-product LFM waveforms. Using exact Doppler compensation (time compression) in the reference channel, the correlation receiver Doppler tolerance was ± 0.6 kn for a sonar with a ratio of center frequency to bandwidth of 5:1 and a processing gain $2WT$ of 10^4. However, for the same correlation receiver and system parameters, the narrow-band approximation would have predicted a Doppler tolerance of ± 150 kn. This substantial difference in Doppler tolerance prediction occurs because the narrow-band correlation loss, which is caused by Doppler mismatch, is governed solely by a frequency shift of the carrier frequency that can be interpreted (Kroszczynski[4]) as an equivalent time shift of the frequency modulation function. Doppler tolerance is then determined by the temporal overlap loss. Using the wideband theory, the actual Doppler tolerance is determined predominantly by the linear frequency-versus-time slope difference between the reference and received LFM signals. As a rule, if the product of the TW product and the fractional bandwidth W/f_c is significantly greater than 1, then the Doppler tolerance must be predicted from the wideband ambiguity function theory.[5] The Doppler tolerance for a narrow-band LFM signal is proportional to the fractional bandwidth W/f_c of the waveform, whereas, for a large TW-product LFM signal, the tolerance is approximately independent of the carrier frequency and is inversely proportional to the TW product.[2,3,6]

The much-reduced Doppler tolerance for large TW-product LFM signals requires the correlation receiver to have a large number of Dopper-compensated reference channels. For this reason, Doppler-invariant waveforms (e.g., linear period modulation, also known as hyperbolic frequency modulation) have been utilized to circumvent the need for multichannel references.[4,7] Because the waveform is invariant to Doppler, there is poor resolution of target velocity. However, both range and velocity resolution can be important to low-frequency active systems that customarily transmit with long repetition periods. Large TW-product LFM signals are Doppler resolvent. At the cost of additional signal processing, both range and velocity can be estimated within the bounds defined by the wideband ambiguity function. Another consideration for large TW-product LFM signals is that their actual acceleration tolerance is high compared to the one predicted by the narrow-band theory, as demonstrated by Kramer.[2] Hence, separate acceleration-processing channels are not required. The correlation receiver output sidelobe levels for the large TW-product LFM signals are higher than the levels of the narrow-band LFM signals. This is to be expected since the volume under the wideband ambiguity function is close to the square of the signal energy as has been shown by Sibul and Titlebaum.[8]

Both Costas[9] and Garber[10] have approached the problem of multipath effects on correlation receivers for large TW-product waveforms by modeling the received signal by a delay-Doppler spreading function. Using the correlation receiver output with no multipath for comparison, the correlation loss for a multipath signal was shown to be dependent on the product of the spreading function and the ambiguity function. When the spreading was less than the resolution of the transmitted signal, the loss was negligible; when it was larger than the resolution of the transmitted signal, the loss varied inversely with the product of the two functions.

Nuttall[11] recently investigated a multitarget correlator response for narrow-band LFM transmitted and reference signals that could differ in amplitude shading and time duration. For rectangular-envelope transmitted and reference signals, constructive and destructive interference of secondary lobes could generate spurious peaks, and Doppler mismatch could broaden the mainlobe of the response. The response for a rectangular-envelope transmitted signal and a Hanning-envelope reference signal was examined for several cases. In general, sidelobe interferences were reduced at the expense of mainlobe broadening. Matched filter discrimination against improperly coded narrow-band signals has been reported by Cohen.[12] Cross-ambiguity functions were developed for signals mismatched in weighting, pulse length, and FM sweep rate. Both unilateral and bilateral Hamming weighting resulted in sidelobe reduction and a corresponding spread in the main ridge of the ambiguity function.

In this article, the delay-Doppler resolution performance of a correlation receiver is analyzed for large TW-product LFM signals in a multipath ocean environment. The reference channels consist of time-compressed (and -expanded) versions of the transmitted pulse. The received signal is represented as a linear summation of returns with arbitrary amplitudes, time delays, and Doppler transformations. A wideband ambiguity function formulation is used to predict the influence of the multipath interference effects on the delay-Doppler resolution performance. A delay-Doppler autocorrelation function is associated with each return and they are translated with respect to each other by their differences in range and velocity. These complex functions are superimposed in magnitude and phase to yield the resultant magnitude of the correlation receiver response. The primary concern in this investigation is estimating range and velocity from the resultant ambiguity surface, which is derived as a function of delay and Doppler. The mathematical approach adopted is similar to Russo and Bartberger's formulation of the ambiguity function for an LFM signal with rectangular envelope.[13] Their analysis technique is extended here to include multiple echo returns and to describe the interference effects on the correlation receiver response. It is assumed that the multi-path/-highlight structure is time invariant and can be represented as a discrete summation of returns. Although the formulation permits arbitrary Doppler compression associated with each return in the echo, emphasis is focused on multi-path/-highlight structures that have the same Doppler. This emphasis is taken to represent low-frequency, long-range echo ranging where the multipath is confined to a narrow angular dispersion in elevation angle and where the target maintains constant aspect angle during the insonification time interval.

Report no. changed (Mar 2006): SM-219-UU

The following analysis demonstrates that for a return from a single-highlight point target, which propagates over a single path, the correlator output envelope is a maximum when the reference signal is exactly matched in delay and Doppler. Target range and radial velocity can be estimated within the bounds defined by the autoambiguity function. When the received signal consists of multiple arrivals, however, the resultant cross-ambiguity surface in delay and Doppler consists of several peaks, and the maximum peak does not necessarily occur at the appropriate Doppler-compensated reference channel. This is due to the constructive/destructive interference of the summation of delay-Doppler autocorrelation functions associated with each return. In general, the maximum peak occurs at a reference channel mismatched in Doppler. A summation technique that identifies the appropriate Doppler reference is proposed; this technique allows the target parameters to be estimated if the signal-to-noise ratio is sufficiently high. Two- and three-dimensional computer modeling is used to display the response envelopes in delay and Doppler.

I. CHARACTERIZATION OF THE TARGET REFLECTED SIGNAL

Consider a transmitted signal $s(t)$ in the form of a modulated carrier,

$$s(t) = a(t)\ \cos[2\pi f_c t + \theta(t)], \tag{1}$$

where $a(t)$ is the amplitude modulation, $\theta(t)$ is the phase modulation, and f_c is the carrier frequency. Although physical systems can only transmit real-valued time signals, it is convenient to use a complex representation of such signals. The physical signal $s(t)$ can be considered as the real part of a complex (analytic) signal $\tilde{s}(t)$: $s(t) = \mathscr{R}[\tilde{s}(t)]$. In principle, the analytic signal can always be found by taking the Hilbert transform of the real signal and adding it as the imaginary part: $\tilde{s}(t) = s(t) + j\hat{s}(t)$. Analogously to (1), the complex analytic signal can be written in the form

$$\tilde{s}(t) = \mu(t)e^{j2\pi f_c t}, \tag{2}$$

where $\mu(t)$ is commonly referred to as the complex envelope. For narrow-band signals, a good approximation of the analytic signal can be obtained by taking the complex envelope in (2) as

$$\mu(t) = a(t)e^{j\theta(t)}. \tag{3}$$

However, for wideband signals the complex envelope generally assumes a much more complicated form. For our purpose, the approximation (3) can be retained even if it is only a poor approximation to the analytic signal.[14] Since complex notation is used exclusively in the following, the complex indicator $\sim$ will be omitted.

Assume that the characteristics of the target are fixed during the time it is illuminated and that it can be modeled as a point target. A point target (as opposed to a distributed target) is one which, if held motionless with respect to the transmitter and receiver, will return an undistorted version of the transmitted signal. The physical effect of source and target relative motion on the reflected signal is a continuous compression (or expansion) of the path length traversed during the transmission. This is mathematically equivalent to a change in time scale and a change in amplitude (to conserve energy) given by

$$\eta_0^{1/2}\, s(\eta_0 t), \tag{4}$$

where $\eta_0 = 1 + \delta_0 \approx 1 - 2V_0/C$ is the Doppler compression factor in which V_0 is the radial velocity of the target and C is the speed of sound in seawater.[15] As defined here, V_0 is positive for an opening target and negative for a closing target. Using complex notation, (4) becomes

$$(1+\delta_0)^{1/2}\mu[(1+\delta_0)t]e^{j2\pi(1+\delta_0)f_c t}. \tag{5}$$

It is seen that the radial velocity has two effects: a compression (or expansion) of the time scale of the complex envelope (including a small amplitude change) and a shift of the carrier frequency. When the signal is narrow band in the sense that the bandwidth W is small compared to the carrier frequency f_c, the first effect can often be neglected. Using this simplified model of Doppler transformation, the reflected signal is

$$\mu(t)\ e^{j2\pi(1+\delta_0)f_c t}. \tag{6}$$

However, even for small fractional bandwidths W/f_c, the compression must be exactly taken into account when the TW product is large. For large fractional bandwidths W/f_c, the amplitude change must always be included. As a rule of thumb, the narrow-band approximation loses its validity when the quantity TW^2/f_c is significantly greater than unity.[5]

The received signal $y(t)$ is taken as an amplitude-attenuated (A_0), time-delayed (τ_0), and Doppler-transformed (η_0) version of the transmitted signal $s(t)$,

$$y(t) = A_0\eta_0^{1/2}\ s[\eta_0(t-\tau_0)], \tag{7}$$

where $\tau_0 = 2R_0/C$ is the round-trip delay (R_0 is the range of the target) in the absence of Doppler effect.

II. RANGE AND RADIAL VELOCITY ESTIMATION

In the previous section, a simple model was presented for the signal returned from a target with particular values of delay and Doppler. The problem of estimating the range and radial velocity of a single target using a correlation receiver is formulated in this section.

A. Correlation receiver

Consider the problem in which τ_0 and η_0 are unknown, nonrandom parameters of a single target that have to be estimated. The range and radial velocity can be estimated by cross correlating the received signal against a set of reference signals. Each of the reference signals is a replica of the transmitted signal that has been artificially Doppler compensated (carrier-frequency-shifted and time-compressed). A significant number of reference channels must be correlated against the received signal to cover the full range of expected target radial velocities. For each combination of delay τ and Doppler η (range-velocity cell), the correlation receiver computes

Report no. changed (Mar 2006): SM-219-UU

$$\Phi(\tau,\eta) = \int_{-\infty}^{+\infty} r_\eta^\dagger(t-\tau)y(t)\,dt, \tag{8}$$

where † denotes complex conjugation and each reference signal $r_\eta(t)$ is a Doppler-compensated version of the transmitted signal $s(t)$,

$$r_\eta(t) = \eta^{1/2}\, s(\eta t). \tag{9}$$

The correlator is followed by a square-law envelope detector. This correlation receiver is illustrated schematically in Fig. 1. Substituting (9) and (7) into (8) is

$$\Phi_0(\tau,\eta) = A_0(\eta\eta_0)^{1/2} \times \int_{-\infty}^{+\infty} s^\dagger(\eta t)s[\eta_0(t+\tau-\tau_0)]\,dt. \tag{10}$$

The maximum of this correlation integral occurs at $\tau = \tau_0$ and $\eta = \eta_0$, that is, when the reference and echo signals are exactly aligned in time delay and Doppler. The maximum is used to detect the target, and its location is used to estimate its range and velocity. The delay parameter τ and the Doppler parameter η of the reference, which result in maximum correlation, provide the delay (range) and Doppler (velocity) estimates. Figure 1 thus depicts the optimum receiver under a wide varity of criteria (such as maximum likelihood), provided that any interference is additive, white, and Gaussian noise.[15]

B. Autoambiguity function

The accuracy, ambiguity, and resolution properties of a particular waveform are described by its ambiguity function. The ambiguity function of a waveform (transmitted signal) can be defined in terms of the output waveform of a (zero-Doppler) matched filter for different Doppler-transformed versions of the input waveform (received signal).[16] This is equivalent to evaluating the correlation function of (8) for $y(t) = s(t)$,

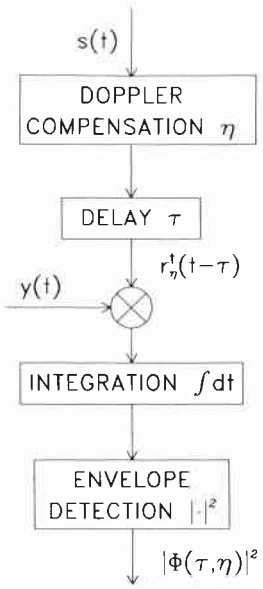

FIG. 1. Basic time-domain replica correlator.

$$\Phi(\tau,\eta) = \eta^{1/2}\int_{-\infty}^{+\infty} s^\dagger(\eta t)\; s(t+\tau)\,dt, \tag{11}$$

which defines the delay-Doppler autocorrelation function of $s(t)$. This correlation integral is maximum and is equal to the total signal energy E when $\tau = 0$ and $\eta = 1$, i.e.,

$$\Phi(0,1) = \int_{-\infty}^{+\infty} |s(t)|^2\,dt = E. \tag{12}$$

The autoambiguity function of $s(t)$ is defined as the magnitude of $\Phi(\tau,\eta)$, normalized to unit peak energy,

$$\chi(\tau,\eta) = |\Psi(\tau,\eta)|, \tag{13}$$

where

$$\Psi(\tau,\eta) = \Phi(\tau,\eta)/E. \tag{14}$$

From the Schwarz inequality, $\chi(\tau,\eta)\leqslant 1$.

III. DOPPLER-MULTIPATH MODEL

In Sec. II A, the structure of an optimum receiver was given for detecting a single target and estimating its range and radial velocity. In order to evaluate the performance of this correlation receiver in the presence of a multipath environment (or a target with multiple highlights), a model is required that accounts for multipath and Doppler.

Consider the situation where the signal returned to the receiver after a single transmission is composed of several echoes. For example, in the case of a single-highlight target, the energy can travel from the source and back along more than one physical path of propagation. Also, a target with a physical structure that includes multiple highlights will return several distinct echoes. It is assumed that the received signal $y(t)$ consists of a sum of M individual echoes $x_i(t)$,

$$y(t) = \sum_{i=1}^{M} x_i(t), \tag{15}$$

where, according to (7), the ith echo is an amplitude-attenuated (A_i), time-delayed (τ_i), and Doppler-transformed (η_i) version of the transmitted signal $s(t)$,

$$x_i(t) = A_i\eta_i^{1/2}\; s[\eta_i(t-\tau_i)]. \tag{16}$$

By using (15) in the integrand of (8), it follows that

$$\Phi(\tau,\eta) = \int_{-\infty}^{+\infty} r_\eta^\dagger(t)\left(\sum_{i=1}^{M} x_i(t+\tau)\right)dt, \tag{17}$$

or, equivalently,

$$\Phi(\tau,\eta) = \sum_{i=1}^{M} \Phi_i(\tau,\eta), \tag{18}$$

where

$$\Phi_i(\tau,\eta) = \int_{-\infty}^{+\infty} r_\eta^\dagger(t)x_i(t+\tau)\,dt. \tag{19}$$

The cross correlation between the reference signal $r_\eta(t)$ and the received signal $y(t)$ appears as a sum of cross-correlation functions between the reference signal $r_\eta(t)$ and each ith individual echo signal $x_i(t)$.

Using (9) and (16) in the integrand of (19) yields

$$\Phi_i(\tau,\eta) = A_i(\eta\eta_i)^{1/2} \times \int_{-\infty}^{+\infty} s^\dagger(\eta t)s[\eta_i(t+\tau-\tau_i)]\,dt, \tag{20}$$

Report no. changed (Mar 2006): SM-219-UU

which is of the same form as (10). The maximum of this correlation integral occurs at $\tau = \tau_i$ and $\eta = \eta_i$, that is, when the reference and ith echo signals are exactly aligned in time delay and Doppler. By introducing the transformation

$$\lambda_i = \tau - \tau_i, \tag{21}$$

(20) can be simplified to

$$\Phi_i(\lambda_i,\eta) = A_i(\eta\eta_i)^{1/2}\int_{-\infty}^{+\infty} s^\dagger(\eta t)s[\eta_i(t+\lambda_i)]\,dt. \tag{22}$$

By further introducing the substitution

$$t' = t + \tfrac{1}{2}\lambda_i \tag{23}$$

to obtain a symmetric expression in λ_i, the need for separate calculations for $\lambda_i < 0$ and $\lambda_i \geqslant 0$ can be avoided. Thus

$$\Phi_i(\lambda_i,\eta) = A_i(\eta\eta_i)^{1/2}\int_{-\infty}^{+\infty} s^\dagger\left[\eta\left(t' - \frac{1}{2}\lambda_i\right)\right] \times s\left[\eta_i\left(t' + \frac{1}{2}\lambda_i\right)\right]dt'. \tag{24}$$

By using the complex notation of (2), the correlation function of (24) can be rewritten in terms of the complex envelope and carrier term of the transmitted signal,

$$\Phi_i(\lambda_i,\eta) = A_i(\eta\eta_i)^{1/2}\,e^{j\pi(\eta_i+\eta)f_c\lambda_i} \times\int_{-\infty}^{+\infty}\mu^\dagger\left[\eta\left(t' - \frac{1}{2}\lambda_i\right)\right]\mu\left[\eta_i\left(t' + \frac{1}{2}\lambda_i\right)\right] \times e^{j2\pi(\eta_i-\eta)f_c t'}\,dt'. \tag{25}$$

In this formulation, we clearly observe the two Doppler effects previously mentioned: shifting of the carrier frequency f_c and time compression of the complex envelope $\mu(t)$. Returning to the narrow-band approximation, we ignore the second effect, which yields the Wigner distribution as a function of μ,

$$\Phi_i(\lambda_i,\eta) = A_i e^{j\pi(\eta_i+\eta)f_c\lambda_i} \times\int_{-\infty}^{+\infty}\mu^\dagger\left(t' - \frac{1}{2}\lambda_i\right)\mu\left(t' + \frac{1}{2}\lambda_i\right) \times e^{j2\pi(\eta_i-\eta)f_c t'}\,dt', \tag{26}$$

where the Doppler compression factors η and η_i in the complex envelopes and the energy conservation factors $\eta^{1/2}$ and $\eta_i^{1/2}$ have been neglected.

Similarly to (13), the cross-ambiguity function of $s(t)$ and $y(t)$, $\chi(\tau,\eta)$, is defined as the magnitude of $\Phi(\tau,\eta)$, normalized to unit peak energy. This function will be used to describe the complete correlation receiver response to a discrete delay and Doppler spread of the transmitted signal as a function of delay and Doppler.

It should be noted that only the distortions due to relative motions of the source and the reflectors are considered; this model does not take into account other distortions which can be induced by scattering from the target and by propagation through the acoustic medium.

IV. APPLICATION TO THE LINEAR FM PULSE

The model developed in Sec. III is now applied to the rectangular-weighted linear FM pulse. In the remaining sections, we refer to the large TW-product case as the case where $TW \gg f_c/W$.

A. Rectangular-weighted LFM pulse

Using complex notation, the (idealized) transmitted LFM pulse is given by

$$s(t) = \mu(t)e^{j2\pi f_c t}, \tag{27}$$

where f_c is the carrier frequency and the complex envelope is

$$\mu(t) = \mathrm{rect}(t/T)e^{j\pi\beta t^2}, \tag{28}$$

in which β is the ratio of the signal bandwidth W to the signal duration T, or sweep rate

$$\beta = \pm W/T. \tag{29}$$

The upper and lower signs indicate an up- and down-sweep, respectively. The "rect" function is defined by

$$\mathrm{rect}(x) = \begin{cases} 1, & \text{if } |x| \leqslant \frac{1}{2}, \\ 0, & \text{otherwise.} \end{cases} \tag{30}$$

The instantaneous frequency varies linearly from $f_c \mp W/2$ to $f_c \pm W/2$ over the time interval $[-T/2, T/2]$ as represented in the time-frequency plane (t, f) of Fig. 2 for the case of an up-sweep in frequency. It is assumed that $W/2 \leqslant f_c$.

B. Narrow-band case

In the case of a narrow-band LFM signal, the Doppler effect can be treated as a pure frequency translation of the entire signal spectrum: The $t-f$ characteristics of the transmitted and received LFM signals are parallel as shown in Fig. 2. The narrow-band formulation given in (26) can be applied. Substitution of $\mu(t')$ from (28) into the integrand of (26) yields, after factoring,

$$\Phi_i(\lambda_i,\eta) = A_i\int_{-\infty}^{+\infty}\mathrm{rect}\left(\frac{t' - \frac{1}{2}\lambda_i}{T}\right)\mathrm{rect}\left(\frac{t' + \frac{1}{2}\lambda_i}{T}\right) \times\exp[j\pi(\eta_i+\eta)f_c\lambda_i] \times\exp\{j2\pi[(\eta_i-\eta)f_c + \beta\lambda_i]t'\}\,dt'. \tag{31}$$

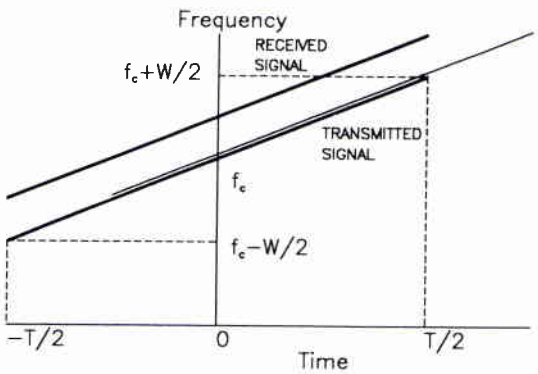

FIG. 2. Mismatched LFM signals: narrow-band case.

Report no. changed (Mar 2006): SM-219-UU

After some calculation, there follows

$$\Phi_i(\lambda_i,\eta) = R_i \exp(j\Theta_i)\operatorname{sinc}(z_i)\,, \tag{32}$$

where

$$z_i = \pi[(\eta_i - \eta)f_c + \beta\lambda_i](T - |\lambda_i|)\,, \tag{32a}$$

$$R_i = A_i(T - |\lambda_i|)\,, \tag{32b}$$

$$\Theta_i = \pi(\eta_i + \eta)f_c\lambda_i\,, \tag{32c}$$

for $|\lambda_i| \leqslant T$. The "sinc" function is defined by

$$\operatorname{sinc}(z) = \sin z/z\,. \tag{33}$$

By letting $i = 1$, $A_1 = 1$, $\tau_1 = 0 (\lambda_1 = \tau)$, $\eta_1 = 1$, and $\eta = 1 + \delta$ in the expressions (32), the delay-Doppler autocorrelation function normalized to unit peak energy may be written as

$$\Psi(\tau,\delta) = R \exp(j\Theta)\operatorname{sinc}(z)\,, \tag{34}$$

where

$$z = \pi(\beta\tau - \delta f_c)(T - |\tau|)\,, \tag{34a}$$

$$R = (T - |\tau|)/T\,, \tag{34b}$$

$$\Theta = \pi(2 + \delta)f_c\tau\,, \tag{34c}$$

for $|\tau| \leqslant T$. The autoambiguity function is given by the magnitude of (34),

$$\chi(\tau,\delta) = R\,|\operatorname{sinc}(z)|\,. \tag{35}$$

A thorough discussion of this function can be found in Ref. 5. From (35), the equation of the main ridge (locus of slowest descent) is obtained by letting $z = 0$ in (34a), to give

$$\delta = (\beta/f_c)\tau\,, \tag{36}$$

which represents a diagonal straight line in the (τ,δ) plane. According to (34b), $\chi(\tau,\delta)$ decreases linearly along the main ridge from $\chi(0,0) = 1$ and reaches half-power (-3 dB) when $R = 1/\sqrt{2}$ and thus when $|\tau_{-3\,\mathrm{dB}}| = 0.3\,T$. From (36), the Doppler tolerance (half-power contour) is given by the Doppler coordinates of the main ridge associated with $\tau_{-3\,\mathrm{dB}}$,

$$\delta_{-3\,\mathrm{dB}} = \pm 0.3W/f_c \tag{37a}$$

or, in knots,

$$V_{-3\,\mathrm{dB}} = \mp 450\,W/f_c\ \mathrm{kn}\,, \tag{37b}$$

where $\delta = -2V/C$ and a value of 3000 kn is assumed for C. Because of the extremely narrow and diagonal nature of the main ridge, it is convenient to visualize the autoambiguity function in a rotated delay-Doppler plane (τ',δ), where the reduced delay variable τ' is defined by

$$\tau' = \tau - (f_c/\beta)\delta\,. \tag{38}$$

In this plane, the projection of the main ridge becomes superimposed on the δ axis. As an example, consider an LFM pulse with the parameters

$$f_c = 900\ \mathrm{Hz}, \quad W = 30\ \mathrm{Hz}, \quad T = 0.5\ \mathrm{s}\,, \tag{39}$$

which is a narrow band ($f_c/W = 30$) and small TW-product ($TW = 15$) signal. From (37a) and (37b), the Doppler tolerance is $|\delta_{-3\,\mathrm{dB}}| = 10^{-2}$ (15 kn). Figure 3 shows the ambiguity surface $\chi(\tau',\delta)$ in the vicinity of the main ridge. The main ridge represents the Doppler-tolerant property of the narrow-band LFM pulse. The correlation loss is due to a time overlap loss, as illustrated in Fig. 2 by the intersection of the (translated) $t - f$ characteristics of the transmitted and received signals. The subsidiary ridges represent the response sidelobes of the correlation receiver. The maximum sidelobe level is 13 dB below the mainlobe.

C. Large *TW*-product case

In the case of a large TW-product LFM signal, the Doppler effect must be treated as a time compression (or expansion) of the transmitted signal: The $t - f$ characteristics of the transmitted and received LFM signals cross as shown in Fig. 4. Hence, the narrow-band approximation loses its validity and the exact formulation of (25) must be used. Substitution of $\mu(t')$ from (28) into the integrand of (25) yields, after factoring,

$$\begin{aligned}\Phi_i(\lambda_i,\eta) = A_i(\eta\eta_i)^{1/2}\int_{-\infty}^{+\infty} &\operatorname{rect}\left(\frac{\eta(t' - \tfrac{1}{2}\lambda_i)}{T}\right)\operatorname{rect}\left(\frac{\eta_i(t' + \tfrac{1}{2}\lambda_i)}{T}\right)\\ &\times\exp\{j\pi[f_c(\eta_i + \eta)\lambda_i + \tfrac{1}{4}\beta(\eta_i^2 - \eta^2)\lambda_i^2]\}\\ &\times\exp(j\pi\{\beta(\eta_i^2 - \eta^2)t'^2 + [2f_c(\eta_i - \eta) + \beta(\eta_i^2 + \eta^2)\lambda_i]t'\})\,dt'\,.\end{aligned} \tag{40}$$

As is shown in Sec. 1 of the Appendix, the above expression can be reduced to a complex form of the Fresnel integral. Two cases must be considered, depending on the sign of the quantity $\beta(\eta_i - \eta)$. The derivation leads to the final result

$$\Phi_i(\lambda_i,\eta) = R_i \exp(j\Theta_i)[F(z_{2,i}) - F(z_{1,i})]\,, \tag{41}$$

where

$$F(z) = C(z) + j\operatorname{sgn}[\beta(\eta_i - \eta)]S(z)\,, \tag{41a}$$

$$z_{1,i} = P_i(t'_{1,i} + Q_i)\,, \tag{41b}$$

$$z_{2,i} = P_i(t'_{2,i} + Q_i)\,, \tag{41c}$$

$$P_i = [2|\beta(\eta_i - \eta)|(\eta_i + \eta)]^{1/2}\,, \tag{41d}$$

$$Q_i = \frac{2f_c(\eta_i - \eta) + \beta(\eta_i^2 + \eta^2)\lambda_i}{2\beta(\eta_i^2 - \eta^2)}\,, \tag{41e}$$

$$R_i = \frac{A_i(\eta\eta_i)^{1/2}}{[2|\beta(\eta_i - \eta)|(\eta_i + \eta)]^{1/2}}\,, \tag{41f}$$

$$\Theta_i = -\pi\frac{[f_c(\eta_i - \eta) - \beta\eta_i\eta\lambda_i]^2}{\beta(\eta_i^2 - \eta^2)}\,, \tag{41g}$$

and the cosine and sine Fresnel integrals are defined by

Report no. changed (Mar 2006): SM-219-UU

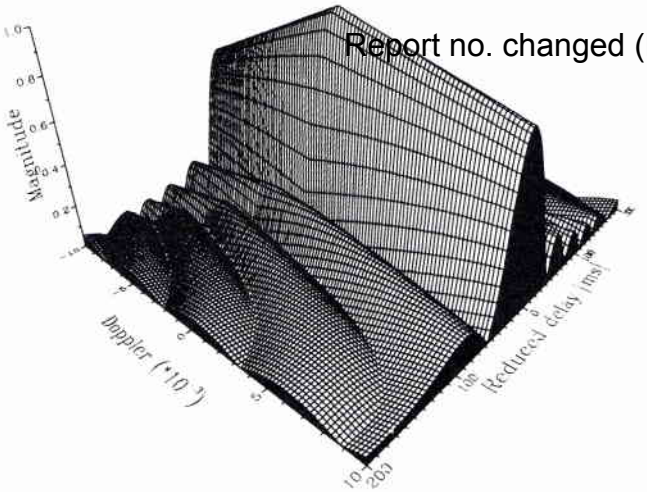

FIG. 3. Autoambiguity surface of a narrow-band LFM: $f_c = 900$ Hz, $W = 30$ Hz, and $T = 0.5$ s.

$$C(z) = \int_0^z \cos\left(\frac{1}{2}\pi\xi^2\right) d\xi , \tag{42a}$$

$$S(z) = \int_0^z \sin\left(\frac{1}{2}\pi\xi^2\right) d\xi , \tag{42b}$$

and the "sgn" function is defined by

$$\operatorname{sgn}(x) = \begin{cases} -1, & \text{if } x < 0, \\ 1, & \text{if } x \geqslant 0. \end{cases} \tag{43}$$

The absolute-value signs under the square root in (41d) are necessary in order to have valid expressions in both cases. The only difference between the two cases is the sign of the imaginary part of the complex Fresnel integral. The ranges of λ_i and the corresponding limits of integration $t'_{1,i}$ and $t'_{2,i}$ to be used in (41b) and (41c) are given in Sec. 3 of the Appendix.

For the special case of a reference signal matched exactly in Doppler to the ith echo signal ($\eta_i = \eta$), the preceding formulas break down and expression (40) becomes

$$\Phi_i(\lambda_i,\eta_i) = A_i\eta_i \int_{-\infty}^{+\infty} \operatorname{rect}[\eta_i(t' - \tfrac{1}{2}\lambda_i)/T)] \times \operatorname{rect}[\eta_i(t' + \tfrac{1}{2}\lambda_i)/T] \times \exp(j2\pi f_c\eta_i\lambda_i)\exp(j2\pi\eta_i^2\beta\lambda_i t')\, dt' , \tag{44}$$

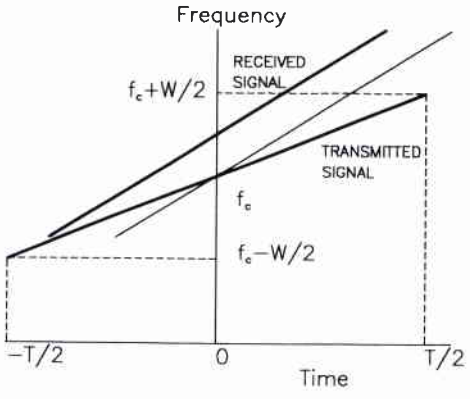

FIG. 4. Mismatched LFM signals: large TW-product case.

which, after calculation (given in Sec. 2 of the Appendix), yields

$$\Phi_i(\lambda_i,\eta_i) = R_i \exp(j\Theta_i)\operatorname{sinc}(z_i) , \tag{45}$$

where

$$z_i = \pi\eta_i\beta\lambda_i(T - \eta_i|\lambda_i|) , \tag{45a}$$

$$R_i = A_i(T - \eta_i|\lambda_i|) , \tag{45b}$$

$$\Theta_i = 2\pi f_c\eta_i\lambda_i , \tag{45c}$$

for $|\lambda_i| \leqslant T/\eta_i$.

By letting $i = 1$, $A_1 = 1$, $\tau_1 = 0$ ($\lambda_1 = \tau$), $\eta_1 = 1$, and $\eta = 1 + \delta$ in the expressions (41) and neglecting δ^2 wherever it appears added to unity, the delay-Doppler autocorrelation function normalized to unit peak energy may be written as

$$\Psi(\tau,\delta) = R \exp(j\Theta)\exp(j\theta)|F(z_2) - F(z_1)| , \tag{46}$$

where

$$F(z) = C(z) + j\operatorname{sgn}(\beta\delta)S(z) , \tag{46a}$$

$$z_1 = P(t_1 + Q) , \tag{46b}$$

$$z_2 = P(t_2 + Q) , \tag{46c}$$

$$P = [2|\beta\delta|(2 + \delta)]^{1/2} , \tag{46d}$$

$$Q = \frac{1}{2 + \delta}\left(\frac{f_c}{\beta} - \frac{1 + \delta}{\delta}\tau\right), \tag{46e}$$

$$R = (1 + \delta)^{1/2}/[T(2|\beta\delta|(2 + \delta))^{1/2}] , \tag{46f}$$

$$\Theta = \pi\frac{[f_c\delta + \beta(1 + \delta)\tau]^2}{\beta\delta(2 + \delta)} , \tag{46g}$$

$$\theta = \operatorname{sgn}(\beta\delta)\tan^{-1}\left(\frac{S(z_2) - S(z_1)}{C(z_2) - C(z_1)}\right). \tag{46h}$$

The ranges of τ and the corresponding limits t_1 and t_2 are given in Sec. 3 of the Appendix. The magnitude of (46) gives the autoambiguity function as

$$\chi(\tau,\delta) = R\,|F(z_2) - F(z_1)| \tag{47a}$$

$$= R\{[C(z_2) - C(z_1)]^2 + [S(z_2) - S(z_1)]^2\}^{1/2} . \tag{47b}$$

For the special case where $\delta = 0$, the expressions (45) must be used and the delay-Doppler autocorrelation function normalized to unit peak energy becomes

$$\Psi(\tau,0) = R \exp(j\Theta)\operatorname{sinc}(z) , \tag{48}$$

where

$$z = \pi\beta\tau(T - |\tau|) , \tag{48a}$$

$$R = (T - |\tau|)/T , \tag{48b}$$

$$\Theta = 2\pi f_c\tau , \tag{48c}$$

for $|\tau| \leqslant T$. The magnitude of (48) is given by

$$\chi(\tau,0) = R\,|\operatorname{sinc}(z)| . \tag{49}$$

The magnitude $\chi(\tau,\delta)$ can be interpreted in terms of the Cornu spiral. In a Cartesian coordinate system, the point of coordinates $[C(z),S(z),z]$ describes a helical spiral whose projection in the complex plane (C,S) is a Cornu spiral, as depicted in Fig. 5. The Cornu spiral is symmetrical with respect to the origin and approaches the point (0.5,0.5) in

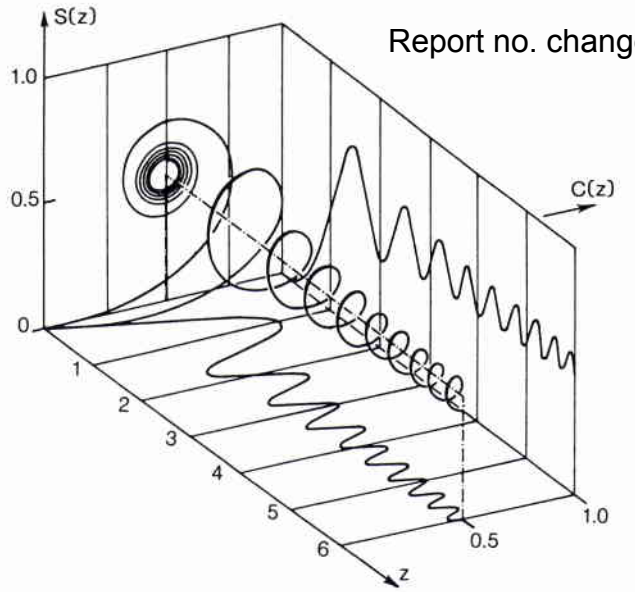

FIG. 5. Fresnel integrals and Cornu spiral.

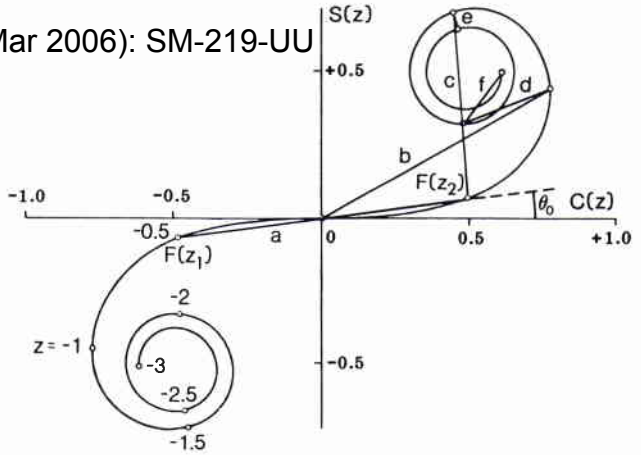

FIG. 6. Geometric interpretation for the magnitude and phase of $\Psi(\tau,\delta)$.

the first quadrant by encircling it an infinite number of times when z tends toward infinity.[17] When small values of Doppler mismatch (i.e., $|\delta| \ll 1$) are considered, the expressions (46d) and (46e) can be further simplified by neglecting δ wherever it appears added to unity, and

$$P = 2|\beta\delta|^{1/2}, \tag{50a}$$

$$Q = \frac{1}{2}\left(\frac{f_c}{\beta} - \frac{\tau}{\delta}\right). \tag{50b}$$

The limits of integration t_1 and t_2 given in Sec. 3 of the Appendix reduce to

$$t_1 = \tfrac{1}{2}(|\tau| - T), \quad t_2 = \tfrac{1}{2}(T - |\tau|), \quad \text{for } |\tau| \leqslant T. \tag{51}$$

Substituting the expressions (50a) and (50b) into (46b) and (46c) yields

$$z_1 = |\beta\delta|^{1/2}(|\tau| - T + f_c/\beta - \tau/\delta), \tag{52a}$$

$$z_2 = |\beta\delta|^{1/2}(T - |\tau| + f_c/\beta - \tau/\delta), \tag{52b}$$

which define the relationship between the (τ,δ) plane and the (z_1,z_2) plane. It is then more convenient to analyze the behavior of χ in the (z_1,z_2) plane independently of the signal parameters f_c, W, and T. Define

$$\Delta z = z_2 - z_1 \tag{53}$$

and

$$\bar{z} = \tfrac{1}{2}(z_2 + z_1), \tag{54}$$

where Δz represents a certain length on the z axis. The arc of Cornu spiral between the end points z_1 and z_2 has this same length. Here, $\bar{z}$ represents the midpoint of this arc. Using (52a) and (52b) gives

$$\Delta z = P(t_2 - t_1) = 2|\beta\delta|^{1/2}(T - |\tau|), \tag{55}$$

$$\bar{z} = PQ = |\beta\delta|^{1/2}(f_c/\beta - \tau/\delta). \tag{56}$$

By using (55), the autoambiguity function (47a) can be rewritten as

$$\chi(z_1,z_2) = \frac{(T - |\tau|)}{T}\,\frac{|F(z_2) - F(z_1)|}{\Delta z}. \tag{57}$$

Hence, $\chi(z_1,z_2)$ is inversely proportional to the length of the arc Δz and is proportional to the length of the chord $|F(z_2) - F(z_1)|$ (straight line joining the end points z_1 and z_2). For small values of τ such that $|\tau| \ll T$, the first term of (57) will be omitted. If Δz (or δ) is fixed and the midpoint $\bar{z}$ approaches the upper or lower limit point of the spiral, then the end points z_1 and z_2 will also approach this limit; the chord becomes progressively smaller, and so does the ambiguity function—which goes through an infinite number of extrema of continually decreasing magnitude. This is illustrated in Fig. 6 for $\Delta z = 1$ and values of $\bar{z}$ increasing from 0 to 2.5 in increments of 0.5 (segments a to f). In fact, χ decreases rapidly when z_1 and z_2 are in the same quadrant of the (C,S) plane (z_1 and z_2 are both positive or negative). Figure 7 shows a contour plot of $\chi(z_1,z_2)$ in the second quadrant of the (z_1,z_2) plane for $|z| \leqslant 5$. The contour lines, given for $0 \leqslant \chi \leqslant 1$ and $\Delta\chi = 0.01$, clearly reveal well-defined peaks and valleys.

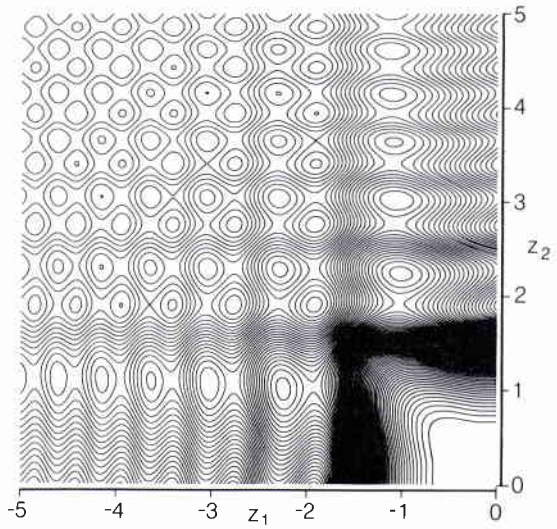

FIG. 7. Contour plot of $\chi(z_1,z_2)$: $0 \leqslant \chi \leqslant 1$, $\Delta\chi = 0.01$.

Report no. changed (Mar 2006): SM-219-UU

We now investigate the extrema (maxima and minima) of χ. That is, we seek those points on the (z_1,z_2) plane that correspond to the peaks and valleys. By taking the derivative of (57), it can be shown that the extrema of $\chi(z_1,z_2)$ satisfy the condition

$$z_2^2 - z_1^2 = 4n\,, \tag{58}$$

where n is a positive or negative integer. By considering n as a parameter, this equation defines a family of hyperbolas centered at the origin with axes oblique to the coordinate axes. The diagonal lines $z_2 = \pm z_1$ corresponding to $n = 0$ are the transverse and conjugate axes of the hyperbolas. In the (τ,δ) plane, the conjugate axis $z_2 = -z_1$ becomes, from (46b)–(46e),

$$\delta = [(\beta/f_c)\tau]/[1 - (\beta/f_c)\tau]\,, \tag{59}$$

which represents the main ridge or "backbone" of $\chi(\tau,\delta)$. Therefore, the main ridge for the large TW-product case is not a straight line as in the narrow-band case [see (36)], but rather is slightly hyperbolic and therefore not symmetric about the origin of the (τ,δ) plane. Similarly to (38), a more appropriate representation can be obtained in the (τ',δ) plane where the reduced delay variable τ' is defined by the transformation

$$\tau' = \tau - (f_c/\beta)[\delta/(1+\delta)]\,. \tag{60}$$

By using the transformation (60) and assuming $|\delta| \ll 1$ and $|\tau| \ll T$, expressions (52a) and (52b) reduce to

$$z_1 = -|\beta\delta|^{1/2}(T + \tau'/\delta)\,, \tag{61a}$$

$$z_2 = |\beta\delta|^{1/2}(T - \tau'/\delta)\,. \tag{61b}$$

By letting $z_1 = 0$ and $z_2 = 0$ in (61a) and (61b), it is seen that each quadrant of the (z_1,z_2) plane is mapped onto a triangular region of the (τ',δ) plane delimited by the diagonal lines

$$\delta = \mp\tau'/T\,. \tag{62}$$

According to the previous discussion, $\chi(\tau',\delta)$ exhibits almost the totality of its energy in the lower and upper triangular regions of the (τ',δ) plane [corresponding to the 2nd and 4th quadrants of the (z_1,z_2) plane]. By solving (61a) and (61b) for τ' and δ, it follows that

$$\tau' = (z_2^2 - z_1^2)/4W = \bar{z}\Delta z/2W\,, \tag{63a}$$

$$\delta = (z_2 - z_1)^2/4WT = \Delta z^2/4WT\,. \tag{63b}$$

From (58) and (63a), the subsidiary peaks are separated in delay by n/W. The amplitudes of the most significant peaks of (57) as well as their exact locations in the (z_1,z_2) plane have been calculated. These values are given in Table I and can be used in conjunction with (63a) and (63b) to determine the delay-Doppler coordinates (τ',δ) of the subsidiary peaks for particular signal characteristics (given values of W and T). The parameter n of the ridge where the maximum lies is also indicated. It will be noted that the amplitudes of these peaks are independent of the signal characteristics. In particular, the four subsidiary peaks that are closest to the origin (highest level) are located at the coordinates

$$(\tau',\delta) = (\pm 1/W, \pm 2.64/WT) \tag{64}$$

TABLE I. Principal maxima of $\chi(z_1,z_2)$.

n	z_1	z_2	$\chi(z_1,z_2)$	$\chi(z_1,z_2)$ (dB)
0	0.00	0.00	1.000	0.0
1	−1.01	2.24	0.525	−5.6
2	−1.06	3.02	0.419	−7.6
0	−2.28	2.28	0.364	−8.8
3	−1.09	3.63	0.362	−8.8
4	−1.10	4.15	0.325	−9.8
1	−2.29	3.04	0.307	−10.3
5	−1.11	4.61	0.298	−10.5
6	−1.12	5.03	0.277	−11.1
2	−2.30	3.65	0.273	−11.3
7	−1.13	5.41	0.260	−11.7

and are only −5.6 dB below the central peak. This has to be compared with the highest sidelobe level of −13 dB of the "sinc" behavior in the narrow-band case. According to the asymptotic evaluation of Harris,[3] the Doppler tolerance (half-power contour) is given by

$$\delta_{-3\,\mathrm{dB}} = \pm 1.74/TW\,, \tag{65a}$$

or, in knots,

$$V_{-3\,\mathrm{dB}} = \mp 2610/TW\ \mathrm{kn}\,. \tag{65b}$$

As an example, consider an LFM pulse with the parameters

$$f_c = 1050\ \mathrm{Hz}, \quad W = 300\ \mathrm{Hz}, \quad T = 5\ \mathrm{s}\,, \tag{66}$$

which is a wideband $(f_c/W = 3.5)$ and large TW-product $(TW = 1500)$ signal. From (64), the actual Doppler tolerance is $|\delta_{-3\,\mathrm{dB}}| \approx 1.2\ 10^{-3}$ (1.74 kn), whereas, according to the narrow-band theory, one would expect the Doppler tolerance to be, from (37), $|\delta_{-3\,\mathrm{dB}}| \approx 8.6\ 10^{-2}$ (129 kn). Figure 8 shows the ambiguity surface $\chi(\tau',\delta)$ in the vicinity of the main ridge. Although such a pulse cannot be treated as a narrow-band signal (since $TW^2/f_c = 43 \gg 1$), it is interesting to consider the autoambiguity function of Fig. 9, obtained by using the narrow-band approximation. By comparing the ambiguity surface in Fig. 8 and its narrow-band

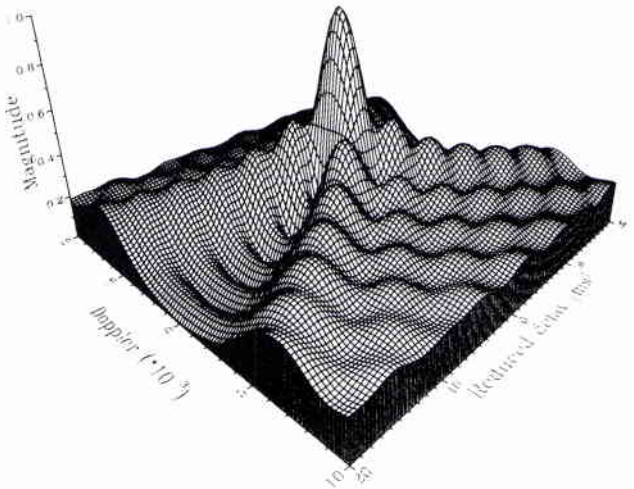

FIG. 8. Autoambiguity surface of a large TW-product LFM: $f_c = 1050$ Hz, $W = 300$ Hz, and $T = 5$ s.

Report no. changed (Mar 2006): SM-219-UU

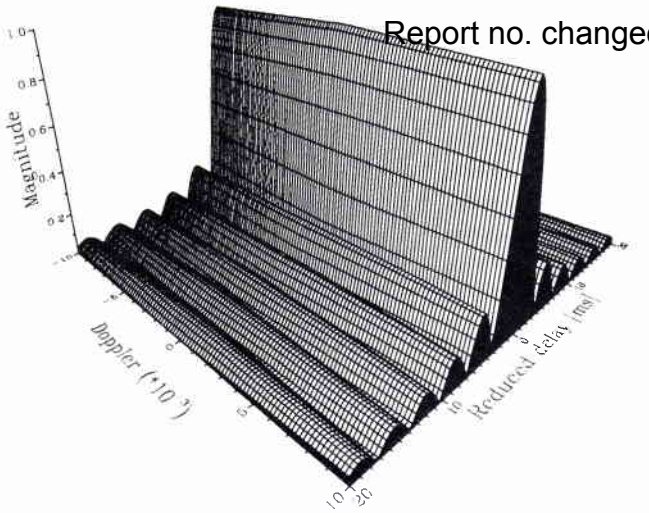

FIG. 9. Function of Fig. 8, but time compression neglected.

counterpart in Fig. 9, it becomes evident that inclusion of the time compression of the complex envelope causes a drastic shortening of the main ridge as well as a completely different sidelobe structure. As illustrated by the translated $t-f$ characteristics of Fig. 4, the total correlation loss is due to both time overlap loss and time-frequency slope difference. The contribution of the latter becomes predominant when TW increases and is responsible for the Doppler-resolvent property of the large TW-product LFM pulse. For comparison, the half-power ambiguity contour and its narrow-band counterpart are sketched in Fig. 10.

The phase behavior of the delay-Doppler autocorrelation function can now be examined. Two phase terms must be considered: the phasor $\exp(j\Theta)$ (including the carrier frequency) and the phasor of the complex Fresnel integral itself $\exp(j\theta)$. The latter can be interpreted directly from the Cornu spiral. The other term will be considered in the next section. Referring back to Fig. 6, it is seen that if $\bar{z}$ is increased for a given Δz, then the angle θ of the chord slowly increases (or decreases for certain large values of Δz) from its initial value θ_0 corresponding to $\bar{z}=0$. If $\bar{z}$ is increased still further, both end points z_1 and z_2 wrap themselves around the spiral, thus causing the chord to rotate more and more rapidly, and the phase of the Fresnel integral does likewise. It is clear that the phase is symmetric about the main ridge, which is defined by the condition $\bar{z}=0$.

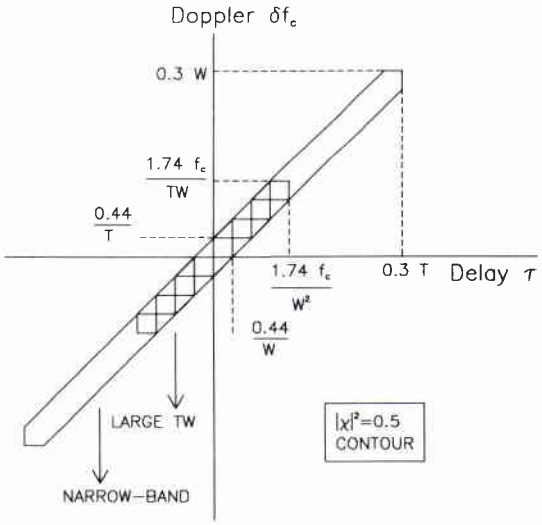

FIG. 10. Half-power ambiguity contour for narrow-band and large TW-product LFM pulses.

V. TWO-PATH PROBLEM

Consider the situation where the transmitted LFM pulse is reflected by a target with a single point highlight and is returned to the receiver through two propagation paths. Assume that the difference of arrival times (including the carrier phase shift) between the two paths is τ_0 and that the Doppler compression factors associated with each path are both equal to η_0. As mentioned before, this situation can occur in low-frequency, long-range echo ranging where only the low-grazing-angle paths have sufficient energy to propagate back to the receiver, so that the differential Doppler between these paths is usually negligible. Note that in the absence of multipath, a nonrotating target with a pair of point highlights will create a similar situation. Without loss of generality, the absolute time delays τ_1 and τ_2 can be chosen symmetrically about the point "$\tau=0$." One then has

$$(\tau_1,\eta_1)=(-\tfrac{1}{2}\tau_0,\eta_0),\quad (\tau_2,\eta_2)=(\tfrac{1}{2}\tau_0,\eta_0)\,. \tag{67}$$

There is one delay-Doppler autocorrelation function $\Phi_i(\tau,\eta)$ associated with each path. The individual functions Φ_1 and Φ_2 are centered on the (τ,η) plane at the coordinates $(-\frac{1}{2}\tau_0,\eta_0)$ and $(\frac{1}{2}\tau_0,\eta_0)$, respectively. According to (18), the resultant delay-Doppler cross-correlation function $\Phi(\tau,\eta)$ will be the sum of Φ_1 and Φ_2. Before superposition, Φ_1 and Φ_2 are weighted with their phase factors, which produces interference between the two functions. For a better understanding of the nature of this interference, we now examine the phase difference between Φ_1 and Φ_2 as a function of delay and Doppler. In order to demonstrate the fundamental role of the Doppler distortion, the narrow-band and large TW-product cases are again compared.

A. Narrow-band case

From (21), (32c), and (67) the instantaneous phase angle Θ_i associated with each path is a linear function of τ,

$$\Theta_i(\tau,\eta)=\pi(\eta_0+\eta)f_c(\tau\pm\tfrac{1}{2}\tau_0),\quad i=1,2\,, \tag{68}$$

where the upper and lower signs stand for Θ_1 and Θ_2, respectively. From (68), the instantaneous frequency $f(\tau)=d\Theta_i(\tau)/d\tau$ is constant for a given η and corresponds to the Doppler-shifted carrier frequency. The phase difference is given by

$$\Delta\Theta(\eta)=\Theta_1-\Theta_2=\pi(\eta_0+\eta)f_c\tau_0\,. \tag{69}$$

Thus the phase difference is constant for a given η. Pure constructive addition of the sidelobes of Φ_1 and Φ_2 will occur when both functions are exactly in phase, that is, when

$$\Delta\Theta=k\,2\pi\,, \tag{70}$$

where k is an integer (positive or negative). Identifying (69) and (70) gives

$$k = \tfrac{1}{2}(\eta_0 + \eta) f_c \tau_0 \,. \tag{71}$$

Report no. changed (Mar 2006): SM-219-UU

For given η_0 and τ_0 and each particular value of k, there exists only one value of η for which both functions are exactly in phase. To simplify, assume that the radial velocity of the target is zero ($\delta = 2V_0/C = 0$), so that $\eta_0 = 1$ and let $\eta = 1 + \delta$. By solving for δ, (71) becomes

$$\delta = 2(k/f_c\tau_0 - 1) \,, \tag{72}$$

which represents horizontal lines in the (τ,δ) plane. Since $|\delta| \ll 1$, only the nearest integers of the quantity $f_c\tau_0$ yield plausible values of δ. As illustrated in Fig. 3, the sidelobe response is smeared with increasing δ and becomes less and less symmetric about the main ridge (magnitude). Also, according to (69), the phase difference slowly varies with δ [since $\Delta\Theta(\delta) \propto (2+\delta)$, where $|\delta| \ll 1$] and remains constant over τ for a given δ (phase). Therefore, no strong local interference can be expected.

B. Large *TW*-product case

As shown before, the phase θ of the Fresnel integral itself is slowly varying in the triangular region where the autoambiguity function assumes significant values and is symmetric about the main ridge. Thus its contribution to the total phase difference between Φ_1 and Φ_2 will always be zero. It suffices, therefore, to consider the phasor $\exp(j\Theta)$ before the Fresnel integral. According to (41g), (45c), and (67), the instantaneous phase angle Θ_i associated with each path is

$$\Theta_i(\tau,\eta) = \begin{cases} 2\pi f_c \eta_0 (\tau \pm \tfrac{1}{2}\tau_0), & \text{if } \eta = \eta_0, \\ -\pi \dfrac{[(\eta_0 - \eta) f_c - \eta_0 \eta \beta (\tau \pm \tfrac{1}{2}\tau_0)]^2}{\beta(\eta_0^2 - \eta^2)}, & \text{otherwise,} \end{cases} \tag{73}$$

where $i = 1,2$ and the upper and lower signs are for Θ_1 and Θ_2, respectively. Except for the special case where $\eta = \eta_0$, the phase is a quadratic function of τ. The phase difference is given by

$$\Delta\Theta(\tau,\eta) = \begin{cases} 2\pi f_c \eta_0 \tau_0, & \text{if } \eta = \eta_0, \\ 2\pi[\eta_0\eta/(\eta_0 + \eta)]\{f_c - [\eta_0\eta/(\eta_0 - \eta)]\beta\tau\}\tau_0, & \text{otherwise.} \end{cases} \tag{74}$$

The phase difference is dependent on both τ and η whereas, in the narrow-band case, it is constant for a given η. Identifying (70) and (74) gives

$$k = \begin{cases} f_c \eta_0 \tau_0, & \text{if } \eta = \eta_0, \\ [\eta_0\eta/(\eta_0 + \eta)]\{f_c - [\eta_0\eta/(\eta_0 - \eta)]\beta\tau\}\tau_0, & \text{otherwise.} \end{cases} \tag{75}$$

For given η_0 and τ_0 and considering k as a parameter, this equation defines a family of curves on the (τ,η) plane, where Φ_1 and Φ_2 are exactly in phase. For simplicity, assume that the radial velocity of the target is zero, so that $\eta_0 = 1$, and let $\eta = 1 + \delta$. Taking the transformation (60) and solving for τ' give

$$\tau' = \frac{\delta}{\beta(1+\delta)}\left(\frac{2+\delta}{1+\delta}\frac{k}{\tau_0} - 2f_c\right). \tag{76}$$

For small values of δ such that $|\delta| \ll 1$, solving for δ,

$$\delta = [\beta/(k/\tau_0 - f_c)]\tau' \,, \tag{77}$$

which represents a family of oblique lines in the (τ',δ) plane, where Φ_1 and Φ_2 are exactly in phase.

As illustrated in Fig. 8, the main ridge of each autoambiguity function is smeared with increasing δ and its energy is split into multiple peaks. For a time delay τ_0 on the order of the inverse bandwidth $1/W$ and a sufficiently large value for the quantity TW^2/f_c compared to unity, there will be two triangular overlap regions (negative and positive δ), in which both individual autoambiguity functions exhibit a significant amount of energy (magnitude). In particular, when

$$\tau_0 = n/W \,, \tag{78}$$

two pairs of subsidiary peaks are superposed in magnitude on the δ axis. These overlapping regions will only fall in realistic Doppler range ($\delta < 10^{-2}$) if the TW product is large ($TW > 10^3$). It is clear that constructive addition of the subsidiary peaks of both functions will occur in the vicinity of the in-phase lines defined by (77) (phase). Only the in-phase lines corresponding to the nearest integers k of the quantity $f_c\tau_0$ will fall in the overlap regions. In particular, when

$$\tau_0 = k/f_c \,, \tag{79}$$

the two individual functions are in phase on the δ axis. Due to the "peaky" behavior of the spreading of these functions, well-defined peaks are likely to appear away from the correct Doppler value. These peaks can be lower or higher than those appearing at the correct delay-Doppler coordinates depending on τ_0. Clearly, for τ_0 much smaller or larger than $1/W$, no spurious peaks can be expected. However, as the number of paths M increases, ith-order overlap regions corresponding to 2,...,$M-1$ and M paths will extend further and further from the τ axis, and spurious peaks are likely to occur in some of these regions. Lower-order regions are more likely to produce spurious peaks than higher-order regions. Spurious peaks will appear in higher-order regions only if a significant number of paths happen to interact constructively in these regions: The crossing points between the in-phase lines are close to each other. The interference effect is illustrated by some examples in the next section.

VI. NUMERICAL EXAMPLES

Report no. changed (Mar 2006): SM-219-UU

The general formulas developed in the previous sections have been programmed for the narrow-band and large TW-product cases. The program allows numerical investigation of any case of interest, in terms of the Doppler-multipath (-multihighlight) response for LFM signals with arbitrary fractional bandwidth and TW product, and for multipath (multihighlight) structure with arbitrary attenuation, Doppler, and delay on each path (highlight). The cross-ambiguity function is plotted as a surface above the delay-Doppler plane, to specify the complete three-dimensional receiver response to the received signal in delay and Doppler.

It does not really matter if the physical situation is multipath or multihighlight, and so "path," "highlight," or "return" are used interchangeably. Although the program permits arbitrary attenuation and Doppler with each return, the attenuation factors are assumed to be equal ($A_i = 1$) and the Doppler compression factors are assumed to be equal and are taken as zero ($\delta_i = 0$). This emphasis is considered representative of low-frequency, long-range echo ranging where the multipath is confined to a narrow angular dispersion in elevation angle and where the target maintains constant aspect angle during the insonification time interval. It is clear that assuming a radial velocity of zero does not affect the generality of the results.

The delay variable is reduced according to (60) in order to show the nature of the contours; otherwise, in the actual diagrams, they are so narrow that they cannot be plotted satisfactorily (see Sec. IV). Two-way propagation (source–target–receiver) is assumed. The Doppler variable represents the ratio of two times the radial velocity to the sound speed; to obtain the radial velocity in knots, it suffices to multiply by 1500. The plots are normalized to the maximum found over the delay-Doppler plane (taken as unity or 0 dB). The same scaling on the delay and Doppler axes is retained for all of the plots to permit easier comparison.

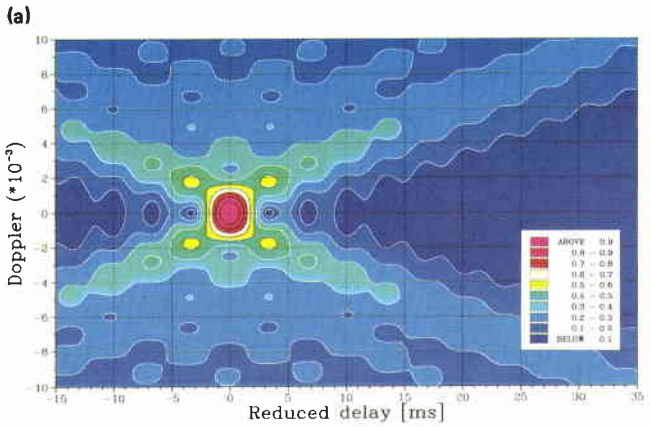

FIG. 11. Function of Fig. 8. (a) Autoambiguity diagram $\chi(\tau',\delta)$: $0 \leqslant \chi \leqslant 1$, $\Delta\chi = 0.1$; (b) correlator outputs $|\Psi(\tau',\delta)|$ for $\delta = 0$ (solid), $|\delta| = 1.76\times10^{-3}$ (dotted), and $|\delta| = 2.77\times10^{-3}$ (dashed); (c) magnitude along the ridges for $\tau' = 0$ ms (solid), $|\tau'| = 3.33$ ms (dotted), and $|\tau'| = 6.67$ ms (dashed).

A. One-path case

Consider the large TW-product LFM pulse of Sec. V where $f_c = 1050$ Hz, $W = 300$ Hz, and $T = 5$ s returned to the receiver through a single path of propagation. Figure 11 (a) shows the autoambiguity diagram that corresponds to horizontal cuts in Fig. 8. The contours at 0.9, 0.7, and 0.5 correspond approximately to -1, -3, and -6 dB, respectively. The main peak (0 dB) and the four subsidiary peaks (-5.6 dB) are clearly evident. Figure 11(b) shows the normalized correlator response for the three values of Doppler given in Table II (see, also, Table I). At zero Doppler (solid line), the highest sidelobe level of the sinc response is -13 dB. At nonzero Doppler values, the mainlobe is split up in multiple peaks. For example, at $|\delta| = 1.76\times10^{-3}$ (dotted line), the mainlobe is split up in two peaks. Figure 11(c) shows the magnitude for the three values of reduced delay given in Table II. The curves represent the magnitude along the "backbone" (solid line) and two subsidiary ridges (dotted and dashed lines). The dotted and dashed curves go to zero at zero Doppler, and corre-

TABLE II. Principal maxima of the autoambiguity function for an LFM pulse with $f_c = 1050$ Hz, $W = 300$ Hz, and $T = 5$ s.

$\lvert\tau'\rvert$ (ms)	$\lvert\delta\rvert\times10^{-3}$	$\lvert\delta\rvert$ (kn)	$\chi(\tau',\delta)$	$\chi(\tau',\delta)$ (dB)
0.00	0.00	0.00	1.000	0.0
3.33	1.76	2.64	0.525	−5.6
6.67	2.77	4.15	0.419	−7.6

spond to the two first nulls of the sinc response (when $|\delta| = 0$).

Report no. changed (Mar 2006): SM-219-UU

B. Two-path case

Figure 12(a) shows the cross-ambiguity diagram for two equal-strength returns separated in time delay by 4 ms. If only the two highest peaks are considered, the response suggests two targets at the same range traveling with opposite radial velocities (opening and closing range) instead of a single standstill target with two highlights (for example). Figure 12(b) shows the correlator output for two particular values of Doppler compensation: The solid line corresponds to a non-Doppler-compensated reference ($\delta = 0$) whereas the dotted line corresponds to the Doppler parameter for which the maximum correlation peak was obtained ($|\delta| = 0.85 \times 10^{-3}$ or $|V| = 1.27$ kn). At the correct Doppler, the two returns are not well resolved, due to bandwidth limitation ($\tau_0 \approx 1/W$), and, in the other channel, the response is reduced to a single peak.

The cross-ambiguity diagram of this pairing, for two returns separated by 10 ms, is given in Fig. 13(a). Since the first nulls in Fig. 11(b) occurred at $\tau' = \pm 3.33$ ms, these two responses are sufficiently separated to clearly see their individual peaks at the correct Doppler [Fig. 13(b)].

Consider a large TW-product LFM pulse as before but with slightly different characteristics: $f_c = 1000$ Hz, $W = 250$ Hz, and $T = 5$ s and now there are two returns

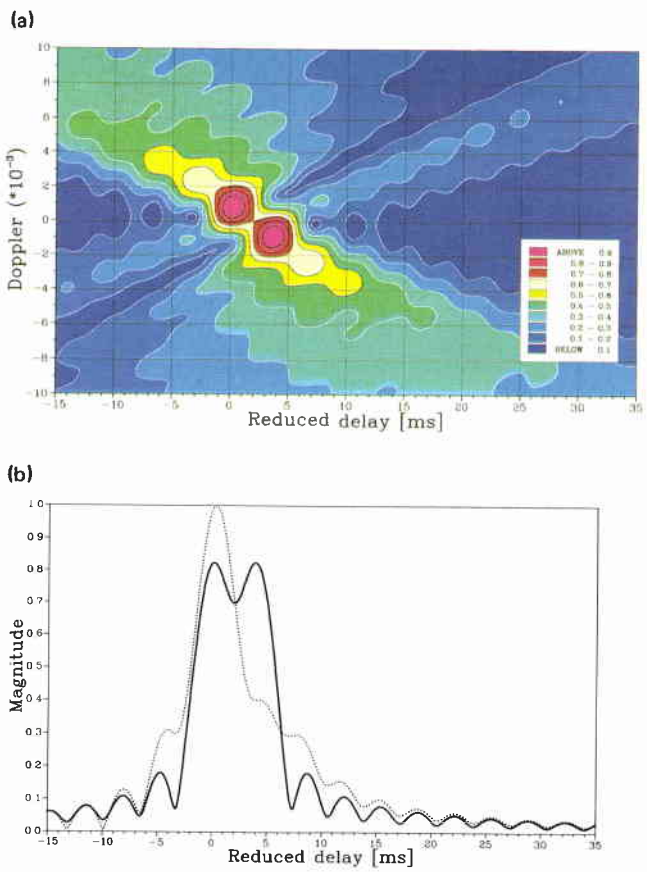

FIG. 12. LFM: $f_c = 1050$ Hz, $W = 300$ Hz, $T = 5$ s; two paths: $A_{1,2} = 1,1$; $\tau_{1,2} = 0,4$ ms; $\delta_{1,2} = 0,0$. (a) Cross-ambiguity diagram $\chi(\tau',\delta)$; (b) correlator outputs $|\Phi(\tau',\delta)|$ for $\delta = 0$ (solid) and $\delta = 0.85 \times 10^{-3}$ (dotted).

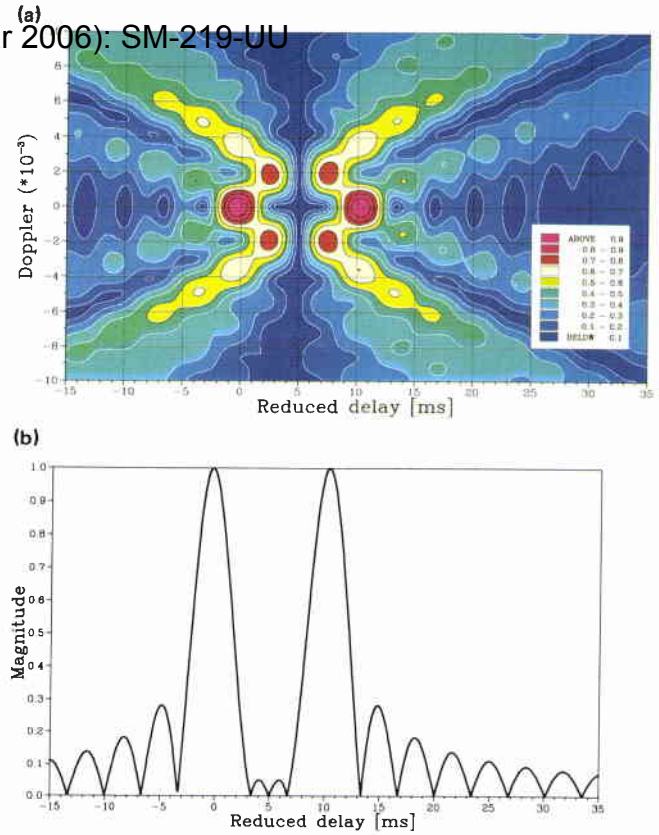

FIG. 13. LFM: $f_c = 1050$ Hz, $W = 300$ Hz, $T = 5$ s; two paths: $A_{1,2} = 1,1$; $\tau_{1,2} = 0,10$ ms; $\delta_{1,2} = 0,0$. (a) Cross-ambiguity diagram $\chi(\tau',\delta)$; (b) correlator output $|\Phi(\tau',\delta)|$ for $\delta = 0$.

separated by 8 ms. With these parameters, the conditions (78) and (79) are fulfilled simultaneously: $\tau_0 = 2/W = 8/f_c = 8$ ms. In this very particular situation, two pairs of subsidiary peaks are exactly superposed (in magnitude), and are added in a purely constructive way (in phase) to produce two spurious peaks at opposite Doppler values [Fig. 14(a)]. Figure 14(b) shows that these peaks (dotted line) have the same amplitude as the two correct peaks at zero Doppler (solid line), where pure constructive addition of the sidelobes occurs as well. This situation yields the maximum errors in the locations of the maxima ($|\delta| = 2.15 \times 10^{-3}$).

C. Four-path case

Consider the same LFM pulse returned to the receiver through four paths of propagation with delays $\tau_1 = 0$ ms, $\tau_2 = 4$ ms, $\tau_3 = 9$ ms, and $\tau_4 = 17$ ms. As is evident in the cross-ambiguity diagram of Fig. 15(a), a well-defined peak is built up away from the correct Doppler. Figure 15(b) shows the maximum correlation peak (squared magnitude) as a function of Doppler. The maximum of this curve appears at $\delta = -2.05 \times 10^{-3}$, and the peak is 2.2 dB above the highest peak at the correct Doppler ($\delta = 0$). The maximum of this curve, that is, the Doppler parameter of the reference channel that results in maximum correlation, is conventionally taken as an estimate of the radial velocity (− 3-kn error). Figure 15(c) shows the correlator output for two particular values of the Doppler compensation: The solid line

Report no. changed (Mar 2006): SM-219-UU

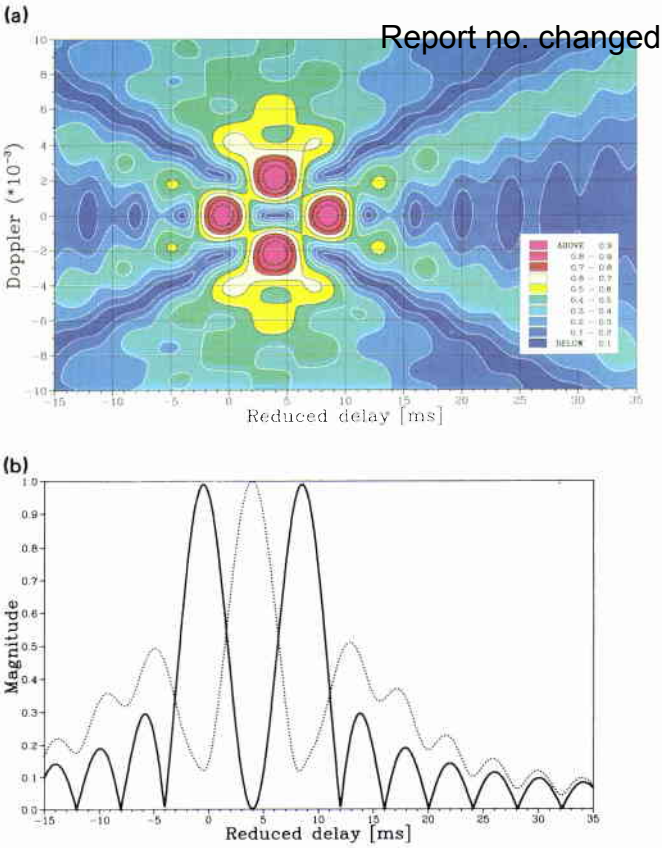

FIG. 14. LFM: $f_c = 1000$ Hz, $W = 250$ Hz, $T = 5$ s; two paths: $A_{1,2} = 1,1$; $\tau_{1,2} = 0,8$ ms; $\delta_{1,2} = 0,0$. (a) Cross-ambiguity diagram $\chi(\tau',\delta)$; (b) correlator outputs $|\Phi(\tau',\delta)|$ for $\delta = 0$ (solid) and $|\delta| = 2.15\times10^{-3}$ (dotted).

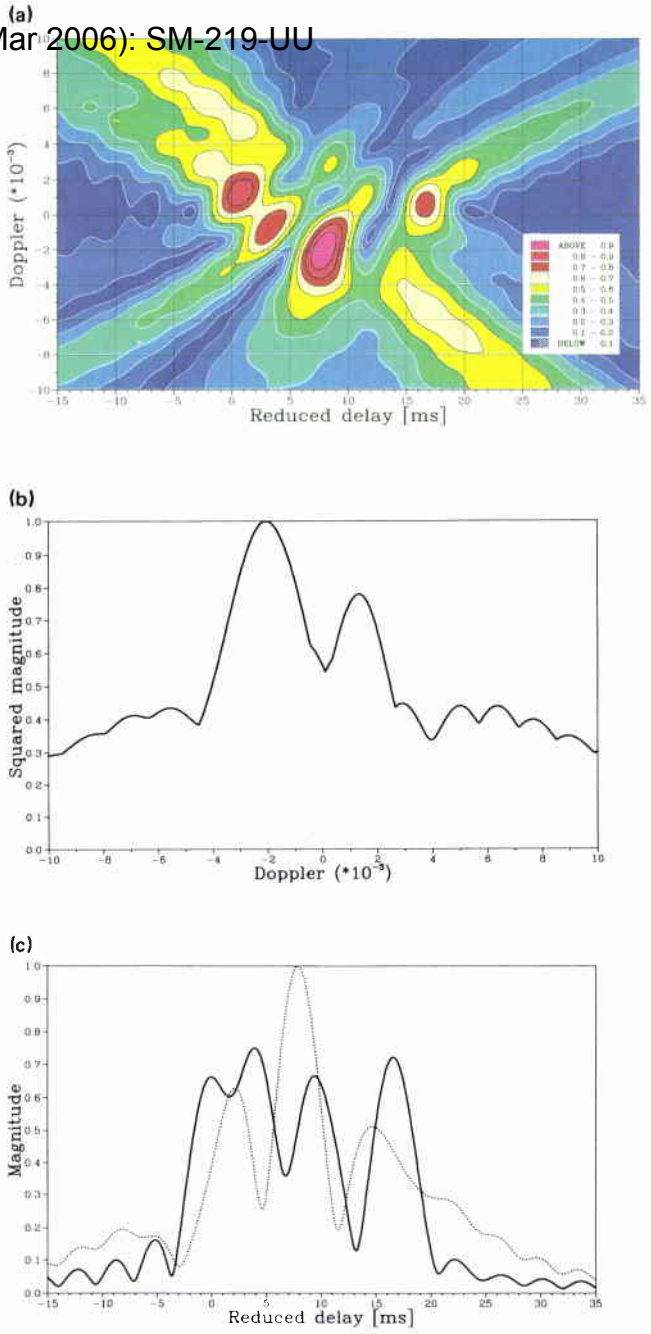

FIG. 15. LFM: $f_c = 1050$ Hz, $W = 300$ Hz, $T = 5$ s; four paths: $A_{1-4} = 1,1,1,1$; $\tau_{1-4} = 0,4,9,17$ ms; $\delta_{1-4} = 0,0,0,0$. (a) Cross-ambiguity diagram $\chi(\tau',\delta)$; (b) maximum correlation peak versus Doppler; (c) correlator outputs $|\Phi(\tau',\delta)|$ for $\delta = 0$ (solid) and $\delta = -2.05\times10^{-3}$ (dotted).

corresponds to a non-Doppler-compensated reference ($\delta = 0$), whereas the dotted line corresponds to the Doppler parameter for which the maximum correlation peak was obtained ($\delta = -2.05\times10^{-3}$). At the correct Doppler, all four arrivals are resolved within the limits defined by the signal bandwidth ($1/W = 3.33$ ms) whereas, at the incorrect Doppler ($\delta = -2.05\times10^{-3}$), the multipath structure is completely missing. To illustrate the effect of time compression, the correlator response has also been calculated without taking into account the Doppler distortion (narrow-band approximation). Figures 16 and 17 show the cross-ambiguity surfaces obtained with and without time compression, respectively. From a comparison of these figures, it becomes evident that inclusion of time compression drastically affects the correlator response.

Consider the four-path case of Fig. 15 but with slightly different arrival times: $\tau_1 = 0$ ms, $\tau_2 = 5$ ms, $\tau_3 = 10$ ms, and $\tau_4 = 20$ ms. Figure 18(a)–(c) is comparable to Fig. 15(a)–(c), respectively. As indicated by Fig. 18 (a), there is again a broad response and numerous spurious peaks where the sidelobes of each highlight happen to interact constructively. The maximum peak occurs at $\delta = -3.6\times10^{-3}$. Error in Doppler is even larger than in the previous case ($-$ 5.4-kn error). Therefore, the exact amplitude and location of the spurious response is strongly dependent on the particular phases of the four arrivals. From these observations it is seen that, for an unknown Doppler, it can be very difficult to extract, from the correlator response, precisely what the detailed multipath (or target highlight) structure is. Also, in most cases there is a gain in signal detectability due to Doppler-mismatched received and reference waveforms: If the target velocity was known but the multipath structure was not, the detection would have been lower at the appropriate reference channel.

D. Gaussian-weighted reference

We now examine the effect of using a weighted replica in the reference channels. A Gaussian weighting function is taken as an example: The complex envelope $\mu(t)$ in (28) is

Report no. changed (Mar 2006): SM-219-UU

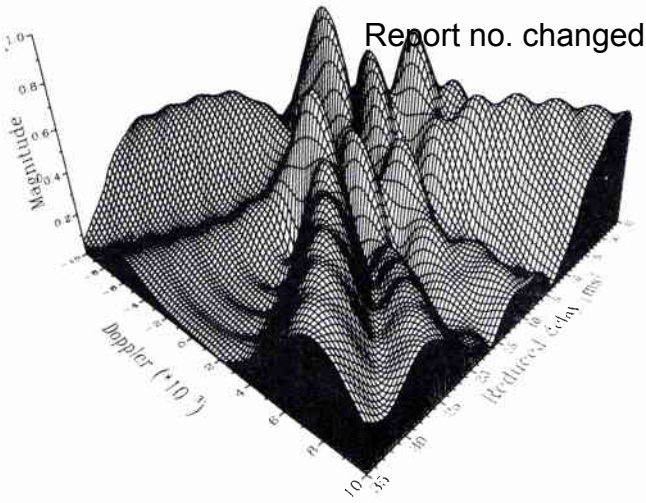

FIG. 16. Cross-ambiguity surface of Fig. 15.

weighted by $\exp(-t^2/2\sigma_0^2)$. The four-path case of Fig. 15 is considered in Fig. 19 for a Gaussian-weighted reference with $|\sigma_0| = T/2$. Comparison with Fig. 15 shows that there is still a pronounced spurious peak at $\delta \approx -2.05\times10^{-3}$. Figure 19(b) shows the correlator outputs (solid and dotted lines) corresponding to Fig. 15(c). When the four-path case of Fig. 19 is reconsidered in Fig. 20 with a smoother weighting function ($|\sigma_0| = T/6$), there are still spurious peaks but they are surrounded by a broader response. Figure 20(b) shows the correlator outputs at $\delta = 0$ (solid line) and $\delta = -3\times10^{-3}$ (dotted line). These examples indicate that there is no significant advantage in using a weighted reference regarding the occurrence of the spurious peaks. However, at the correct Doppler matching, the sidelobe levels are reduced at the expense of broadened mainlobe response and a loss in detectability.

E. Summation technique

We now describe a technique that can be used to identify the appropriate Doppler reference channel to allow the target parameters (range and radial velocity) to be estimated. As a by-product, the detailed multipath (multihighlight) structure can also be extracted within the limits defined by the signal bandwidth. The basic idea is simple: Even if constructive interference occurring somewhere in the delay-Doppler plane produces a very strong false peak, its energy will always be smaller than the total energy that can be retrieved from the individual peaks at the correct Doppler channel. The technique follows naturally: For each Doppler channel, the energies (squared magnitude) of the peaks in the correlator output that exceed a certain threshold are summed; the results are plotted as a function of the Doppler parameter and the maximum of the curve is taken as an estimate of the radial velocity. All the correlator outputs must

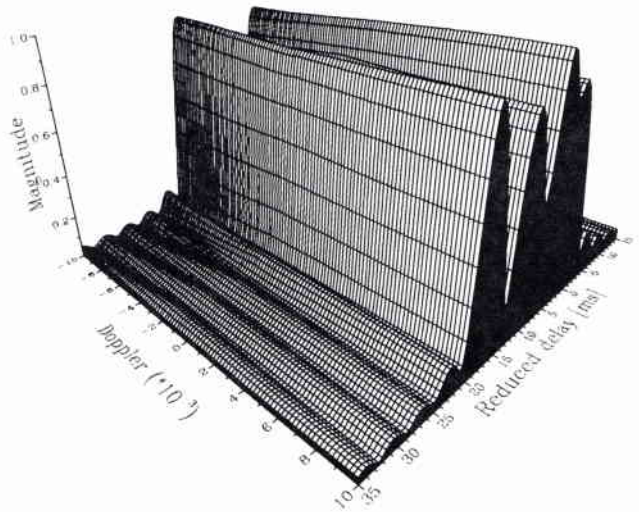

FIG. 17. Function of Fig. 16, but time compression neglected.

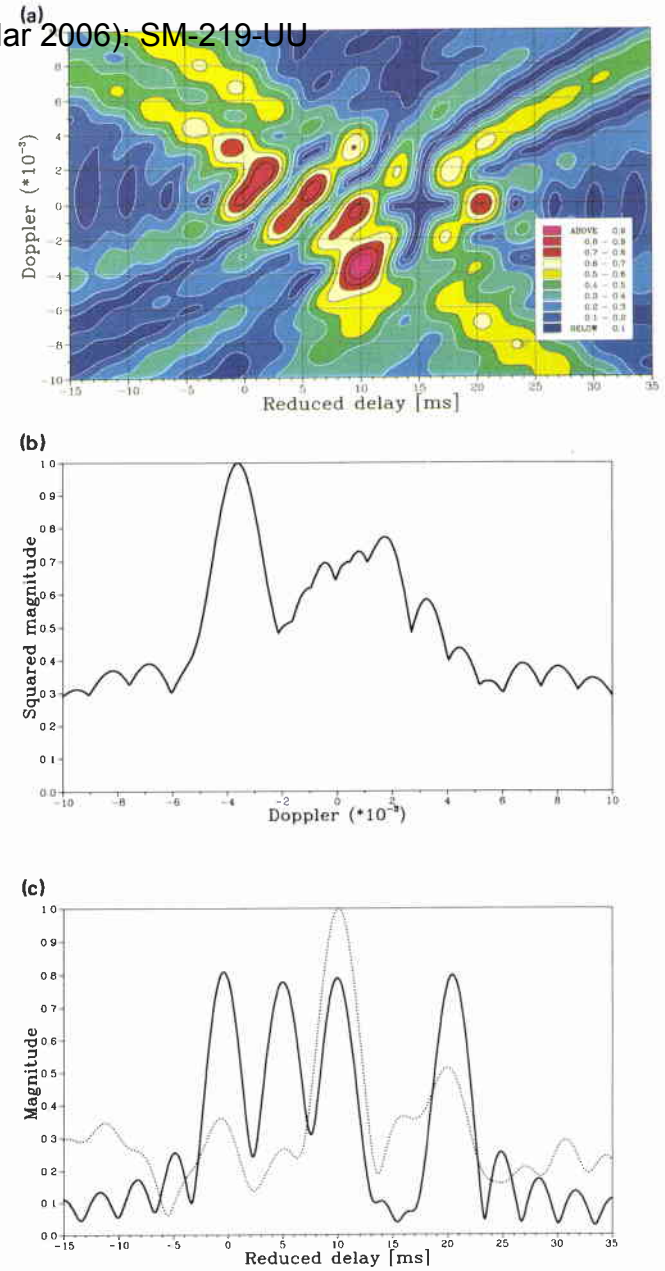

FIG. 18. LFM: $f_c = 1050$ Hz, $W = 300$ Hz, $T = 5$ s; four paths: $A_{1\text{-}4} = 1,1,1,1$; $\tau_{1\text{-}4} = 0,5,10,20$ ms; $\delta_{1\text{-}4} = 0,0,0,0$. (a) Cross-ambiguity diagram $\chi(\tau',\delta)$; (b) maximum correlation peak versus Doppler; (c) correlator outputs $|\Phi(\tau',\delta)|$ for $\delta = 0$ (solid) and $\delta = -3.60\times10^{-3}$ (dotted).

Report no. changed (Mar. 2006): SM-219-UU

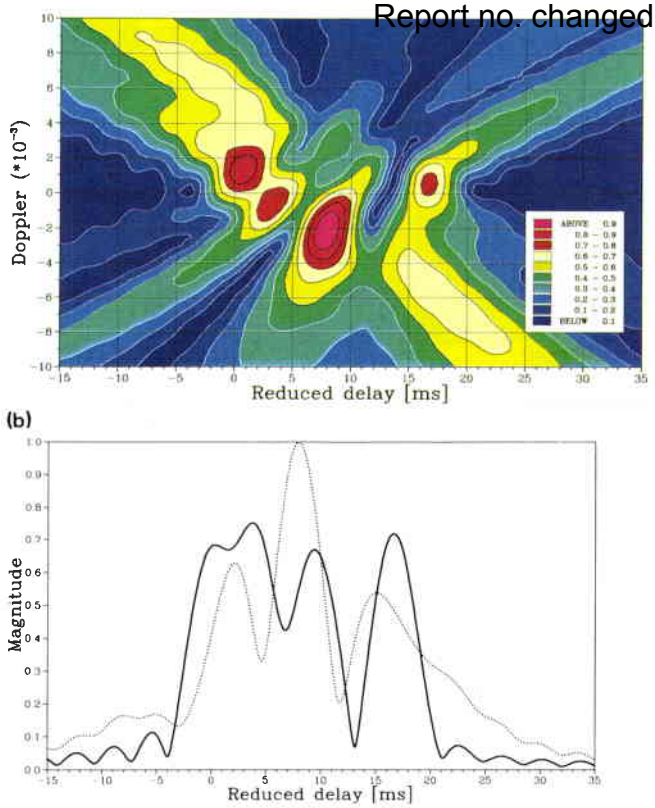

FIG. 19. Function of Fig. 15, but Gaussian-weighted reference with $|\sigma_0| = T/2$. (a) Cross-ambiguity diagram $\chi(\tau',\delta)$; (b) correlator outputs $|\Phi(\tau',\delta)|$ for $\delta = 0$ (solid) and $\delta = -2\times10^{-3}$ (dotted).

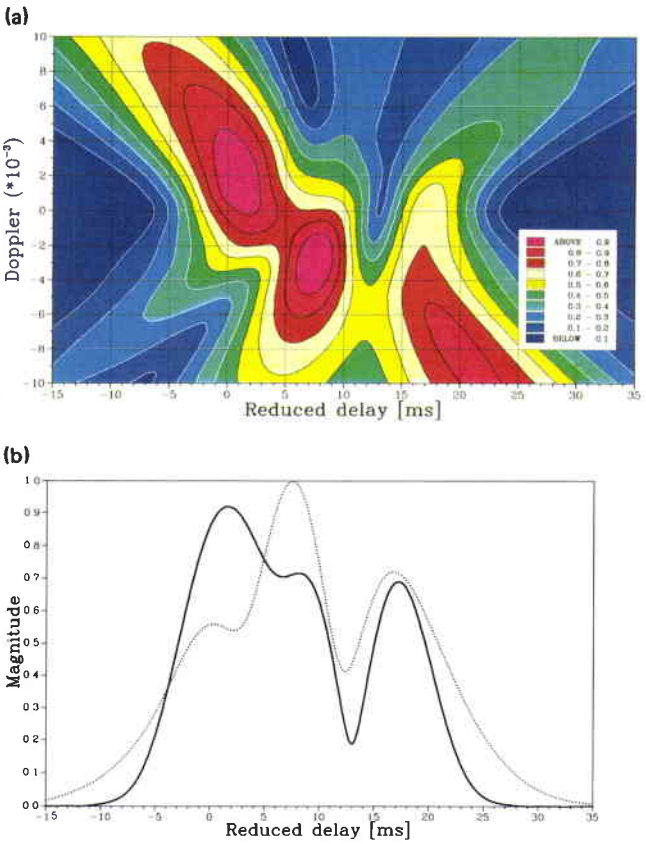

FIG. 20. Function of Fig. 19, but Gaussian-weighted reference with $|\sigma_0| = T/6$. (a) Cross-ambiguity diagram $\chi(\tau',\delta)$; (b) correlator outputs $|\Phi(\tau',\delta)|$ for $\delta = 0$ (solid) and $\delta = -3\times10^{-3}$ (dotted).

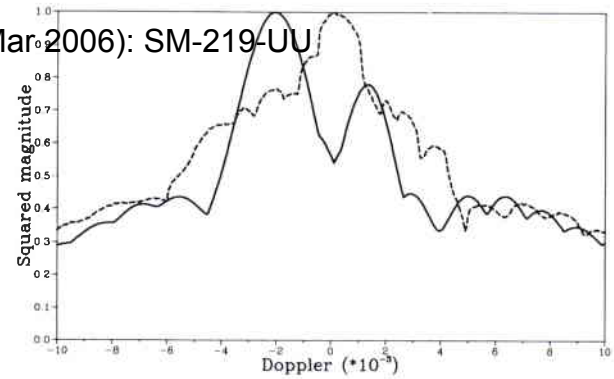

FIG. 21. Maximum correlation peak (solid) and sum of the correlation peaks (dashed) versus Doppler [see Fig. 15(b)].

be normalized to the maximum correlation peak found across all the Doppler channels. Figures 21 and 22 correspond, respectively, to Figs. 15(b) and 18(b) of the two four-path cases that have been considered previously. The solid line represents the conventional Doppler localization process and the dashed line represents the summation technique. It is seen that, in both cases, the correct Doppler was perfectly identified. The selected threshold was 3 dB below the maximum correlation peak. As is to be expected, the technique relies on the selection of an appropriate threshold and, although it works very well in a noise-free environment, it is clear that such a technique is limited by the signal-to-noise ratio. However, the technique can be applied after detection if the signal-to-noise ratio is sufficiently high.

VII. CONCLUSIONS

The analysis given here has demonstrated that for a return from a single-highlight point target, which propagates over a single path, the correlator output envelope is a maximum when the reference signal is exactly matched in delay and Doppler. Target range and radial velocity can be estimated within the bounds defined by the ambiguity function. When the received signal consists of multiple arrivals, however, the resultant cross-ambiguity surface in delay and Doppler consists of several peaks, and the maximum peak does not generally occur at the appropriate Doppler-com-

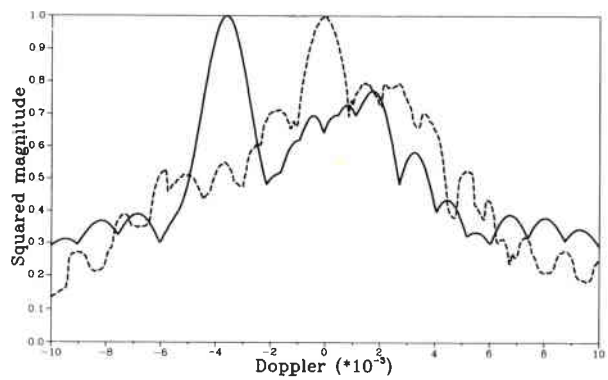

FIG. 22. Maximum correlation peak (solid) and sum of the correlation peaks (dashed) versus Doppler [see Fig. 18(b)].

pensated reference channel. This is due to the constructive/destructive interference of the summation of delay-Doppler autocorrelation functions associated with each return. It has been shown that spurious peaks occur particularly in multipath environments where the relative arrival times are of the order of the inverse bandwidth. Errors in the locations and amplitudes of the peaks increase with the number of paths (highlights). Differences as large as ± 5 kn in radial velocity and $+3$ dB in the correlation peak have been found. Therefore, echo detection can be significantly improved by using a "fine-grained" bank of Doppler-compensated references even if the radial velocity of the target is known.

For the case of large TW-product signals, there is no apparent advantage in using a weighted reference channel to minimize the occurrence of false peaks.

The summation technique that has been described identifies the correct Doppler reference that allows the target parameters (and the multipath structure) to be estimated if the signal-to-noise ratio is sufficiently high.

Report no changed (Mar 2006): SM-219-UU

The generality of the program allows the user to numerically investigate his own cases of interest, in terms of the Doppler-multipath (or-highlight) response for LFM signals with arbitrary fractional bandwidth and TW product, and for multipath (multihighlight) structure with arbitrary attenuation factors, Doppler shifts, and arrival times. For investigation purposes, the program is computationally much more efficient than any simulation program that has to correlate a received signal against a very "fine-grained" bank of Doppler-compensated references.

APPENDIX: DERIVATION OF $\Phi_i(\lambda_i,\eta)$ FOR LARGE TW-PRODUCT LFM PULSES

1. Mismatched Doppler

From (40), the delay-Doppler autocorrelation when $\eta_i \neq \eta$ is given by

$$\Phi_i(\lambda_i,\eta) = A_i(\eta\eta_i)^{1/2}\exp\{j\pi[f_c(\eta_i+\eta)\lambda_i + \tfrac{1}{4}\beta(\eta_i^2-\eta^2)\lambda_i^2]\} \times\int_{t'_{1,i}}^{t'_{2,i}} \exp(j\pi\{\beta(\eta_i^2-\eta^2)t'^2 + [2f_c(\eta_i-\eta)+\beta(\eta_i^2+\eta^2)\lambda_i]t'\})\,dt' , \tag{A1}$$

where the limits of integration $t'_{1,i}$ and $t'_{2,i}$ are determined by the overlap region of the two "rect" functions that are discussed in Sec. 3 of this Appendix. This expression can be reduced to a form of the Fresnel integral; depending on the sign of the quantity $\beta(\eta_i-\eta)$, two cases must be considered separately. Introducing the substitutions

$$P_i = [2|\beta(\eta_i-\eta)|(\eta_i+\eta)]^{1/2} \tag{A2}$$

and

$$Q_i = [2f_c(\eta_i-\eta)+\beta(\eta_i^2+\eta^2)\lambda_i]/[2\beta(\eta_i^2-\eta^2)] \tag{A3}$$

into the integrand of (A1) gives

$$\Phi_i(\lambda_i,\eta) = A_i(\eta\eta_i)^{1/2}\exp\{j\pi[f_c(\eta_i+\eta)\lambda_i + \tfrac{1}{4}\beta(\eta_i^2-\eta^2)\lambda_i^2]\} \times\int_{t'_{1,i}}^{t'_{2,i}} \exp\left(\pm j\frac{1}{2}\pi P_i^2(t'^2+2Q_it')\right)dt' , \tag{A4}$$

where $\pm$ takes the sign of $\beta(\eta_i-\eta)$. Absolute-value signs are assigned to $\beta(\eta_i-\eta)$ in (A2) in order to have valid expressions for both cases. The only difference between the two cases is the sign of the imaginary exponent in the integrand. After some algebraic manipulations, there follows

$$\Phi_i(\lambda_i,\eta) = A_i(\eta\eta_i)^{1/2}\exp(j\theta_i) \times\int_{t'_{1,i}}^{t'_{2,i}} \exp\left(\pm j\frac{1}{2}\pi[P_i(t'+Q_i)]^2\right)dt' , \tag{A5}$$

where

$$\theta_i = -\pi[f_c(\eta_i-\eta)-\beta\eta_i\eta\lambda_i]^2/[\beta(\eta_i^2-\eta^2)] . \tag{A6}$$

By letting

$$z = P_i(t'+Q_i) \tag{A7'}$$

and

$$dz = P_i\,dt' , \tag{A7''}$$

(A5) yields

$$\Phi_i(\lambda_i,\eta) = R_i\exp(j\theta_i)\int_{z_{1,i}}^{z_{2,i}} \exp\left(\pm j\frac{1}{2}\pi z^2\right)dz , \tag{A8}$$

where

$$z_{1,i} = P_i(t'_{1,i}+Q_i) , \tag{A9'}$$

$$z_{2,i} = P_i(t'_{2,i}+Q_i) , \tag{A9''}$$

and

$$R_i = A_i(\eta\eta_i)^{1/2}/P_i . \tag{A10}$$

2. Special case of matched Doppler

From (44), the delay-Doppler autocorrelation when $\eta_i = \eta$ is given by

$$\Phi_i(\lambda_i,\eta_i) = A_i\eta_i\exp(j2\pi f_c\eta_i\lambda_i) \times\int_{t'_{1,i}}^{t'_{2,i}} \exp(j2\pi\eta_i^2\beta\lambda_i t')\,dt' , \tag{A11}$$

where $t'_{1,i}$ and $t'_{2,i}$ have the limits that are discussed in Sec. 3 of this Appendix. Integration yields

TABLE AI. Range of time delay and limits of integration of $\Phi_i(\lambda_i,\eta)$.

Report no. changed (Mar 2006): SM-219-UU

Range of λ_i	$t'_{1,i}$	$t'_{2,i}$
Case I: $\eta_i \neq \eta$		
$-\frac{T}{2}\left(\frac{\eta_i+\eta}{\eta_i\eta}\right) \leqslant \lambda_i < -\frac{T}{2}\left\lvert\frac{\eta_i-\eta}{\eta_i\eta}\right\rvert$	$-\frac{\lambda_i}{2}-\frac{T}{2\eta_i}$	$\frac{\lambda_i}{2}+\frac{T}{2\eta}$
$-\frac{T}{2}\left\lvert\frac{\eta_i-\eta}{\eta_i\eta}\right\rvert \leqslant \lambda_i \leqslant \frac{T}{2}\left\lvert\frac{\eta-\eta_i}{\eta_i\eta}\right\rvert$	$\frac{\lambda_i}{2}-\frac{T}{2\eta}$	$\frac{\lambda_i}{2}+\frac{T}{2\eta}$ if $\eta_i<\eta$
	$-\frac{\lambda_i}{2}-\frac{T}{2\eta_i}$	$-\frac{\lambda_i}{2}+\frac{T}{2\eta_i}$ if $\eta_i>\eta$
$\frac{T}{2}\left\lvert\frac{\eta-\eta_i}{\eta_i\eta}\right\rvert < \lambda_i \leqslant \frac{T}{2}\left(\frac{\eta_i+\eta}{\eta_i\eta}\right)$	$\frac{\lambda_i}{2}-\frac{T}{2\eta}$	$-\frac{\lambda_i}{2}+\frac{T}{2\eta_i}$
Case II: $\eta_i = \eta$		
$\lvert\lambda_i\rvert \leqslant \frac{T}{\eta_i}$	$\left\lvert\frac{\lambda_i}{2}\right\rvert-\frac{T}{2\eta_i}$	$-\left\lvert\frac{\lambda_i}{2}\right\rvert+\frac{T}{2\eta_i}$

$$\Phi_i(\lambda_i,\eta_i) = A_i\eta_i \exp(j2\pi f_c\eta_i\lambda_i)(1/\pi\eta_i^2\beta\lambda_i) \times [\exp(j2\pi\eta_i^2\beta\lambda_i t')/2j]_{t'_{1,i}}^{t'_{2,i}}, \quad \text{(A12)}$$

and substituting $t'_{1,i}$ and $t'_{2,i}$ by the expressions given in case II of Table AI gives, after simplification,

$$\Phi_i(\lambda_i,\eta_i) = A_i \exp(j2\pi f_c\eta_i\lambda_i)(T-\eta_i|\lambda_i|) \times \frac{\sin[\pi\eta_i\beta\lambda_i(T-\eta_i|\lambda_i|)]}{\pi\eta_i\beta\lambda_i(T-\eta_i|\lambda_i|)}. \quad \text{(A13)}$$

3. Range of time delay and limits of integration

The limits of integration of the correlation integrals (A1) and (A11) are now determined. The integrand is zero, except when the echo and reference signals overlap. Let T_i and T_r be the durations of the ith echo and reference signals, respectively. With Doppler compensation, these limits become

$$T_i = T/\eta_i, \quad T_r = T/\eta. \quad \text{(A14)}$$

Two specific cases arise depending on whether the duration of the reference signal is smaller or greater than the duration of the echo signal: These are cases 1 and 2. A special case, case 3, corresponds to the situation where both the reference and echo signals have the same duration. Because of complications arising from the time compression (or expansion) of these signals, three subcases must be considered for each case except for case 3, which reduces to two subcases. Cases 1 and 2 are illustrated in Fig. A1, where the lower and higher

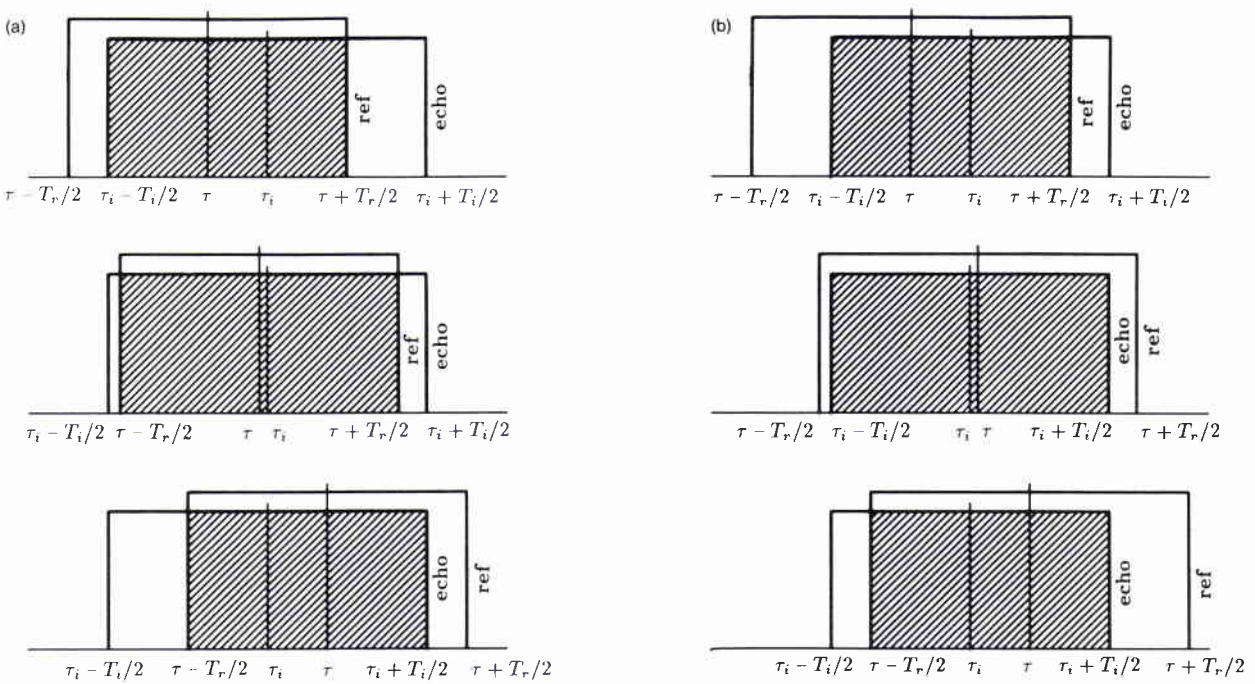

FIG. A1. Limits of integration of the delay-Doppler autocorrelation function. (a) Case 1: $T_r < T_i$; (b) case 2: $T_r > T_i$.

rectangles represent the envelopes of the echo and reference signals, respectively. By moving the reference signal along the time axis and using the relations (21) and (23) from the main text, one obtains the ranges of time delay λ_i and the corresponding limits of integration $t'_{1,i}$ and $t'_{2,i}$. Using absolute value signs and reintroducing explicitly the Doppler compression factors η_i and η, we combine cases 1 and 2 as case I, and case 3 becomes case II (see Table AI).

Report no changed (Mar 2006): SM-219-UU

[1]P. M. Woodward, *Probability and Information Theory with Applications to Radar* (Pergamon, London, 1953).

[2]S. A. Kramer, "Doppler and Acceleration Tolerances of High-gain, Wideband Linear FM Correlation Sonars," Proc. IEEE **55**, 627–636 (1967).

[3]B. Harris and S. A. Kramer, "Asymptotic Evaluation of the Ambiguity Functions of High-gain FM Matched Filter Sonar Systems," Proc. IEEE **56**, 2149–2157 (1968).

[4]J. J. Kroszczynski, "Pulse Compression by Means of Linear-period Modulation," Proc. IEEE **57**, 1260–1266 (1969).

[5]R. L. Mitchell and A. W. Rihaczek, "Matched Filter Responses of the Linear FM Waveform," IEEE Trans. Aerosp. Electron. Syst. **4**, 417–432 (1968).

[6]T. H. Glisson, C. I. Black, and A. P. Sage, "On Sonar Signal Analysis," IEEE Trans. Aerosp. Electron. Syst. **6**, 37–50 (1970).

[7]R. A. Altes and E. L. Titlebaum, "Bat Signals as Optimally Doppler Tolerant Waveforms," J. Acoust. Soc. Am. **48**, 1014–1020 (1970).

[8]L. H. Sibul and E. L. Titlebaum, "Volume Properties for the Wideband Ambiguity Function," IEEE Trans. Aerosp. Electron. Syst. **17**, 83–87 (1981).

[9]J. P. Costas, "Medium Constraints on Sonar Design and Performance," Tech. Inf. Ser. Rep. R65EMH33, General Electric Company, Syracuse, NY (1965).

[10]S. M. Garber, "High Resolution Sonar Signals in a Multipath Environment," IEEE Trans. Aerosp. Electron. Syst. **2**, 431–440 (1966).

[11]A. H. Nuttall, "Linear-FM Correlator Response for Multiple Targets; Mismatched Reference and Signal Amplitude Modulations," Tech. Rep. 7543, Naval Underwater Systems Center, New London, CT (1985).

[12]S. A. Cohen, "Cross-ambiguity Function for a Linear FM Pulse Compression Radar," IEEE Trans. Electromagn. Compat. **14**, 85–91 (1972).

[13]D. M. Russo and C. L. Bartberger, "Ambiguity Diagram for Linear FM Sonar," J. Acoust. Soc. Am. **38**, 183–190 (1965).

[14]A. W. Rihaczek, "Delay-Doppler Ambiguity Function for Wideband Signals," IEEE Trans. Aerosp. Electron. Syst. **3**, 705–711 (1967).

[15]H. L. Van Trees, *Detection, Estimation and Modulation Theory—Part III* (Wiley, New York, 1971).

[16]A. I. Sinsky and C. P. Wang, "Standardization of the Definition of the Radar Ambiguity Function," IEEE Trans. Aerosp. Electron. Syst. **10**, 532–534 (1974).

[17]A. Sommerfeld, *Optics, Lectures on Theoretical Physics, Vol. IV* (Academic, New York, 1967).

Initial Distribution for SM-219

Ministries of Defence	
JSPHQ Belgium	2
DND Canada	10
CHOD Denmark	8
MOD France	8
MOD Germany	15
MOD Greece	11
MOD Italy	10
MOD Netherlands	12
CHOD Norway	10
MOD Portugal	5
MOD Spain	2
MOD Turkey	5
MOD UK	20
SECDEF US	60
NATO Authorities	
Defence Planning Committee	3
NAMILCOM	2
SACLANT	3
SACLANTREPEUR	1
CINCWESTLANT/ COMOCEANLANT	1
COMSTRIKFLTANT	1
CINCIBERLANT	1
CINCEASTLANT	1
COMSUBACLANT	1
COMMAIREASTLANT	1
SACEUR	2
CINCNORTH	1
CINCSOUTH	1
COMNAVSOUTH	1
COMSTRIKFORSOUTH	1
COMEDCENT	1
COMMARAIRMED	1
CINCHAN	3
SCNR for SACLANTCEN	
SCNR Belgium	1
SCNR Canada	1
SCNR Denmark	1
SCNR Germany	1
SCNR Greece	1
SCNR Italy	1
SCNR Netherlands	1
SCNR Norway	1
SCNR Portugal	1
SCNR Turkey	1
SCNR UK	1
SCNR US	2
SECGEN Rep. SCNR	1
NAMILCOM Rep. SCNR	1
National Liaison Officers	
NLO Canada	1
NLO Denmark	1
NLO Germany	1
NLO Italy	1
NLO UK	1
NLO US	1
NLR to SACLANT	
NLR Belgium	1
NLR Canada	1
NLR Denmark	1
NLR Germany	1
NLR Greece	1
NLR Italy	1
NLR Netherlands	1
NLR Norway	1
NLR Portugal	1
NLR Turkey	1
NLR UK	1
Total external distribution	236
SACLANTCEN Library	10
Stock	34
Total number of copies	280